THE GROWTH OF VANADIUM DIOXIDE THIN FILMS BY MAGNETRON SPUTTERING TECHNIQUE AND TERAHERTZ WAVE MODULATION CHARACTERISTICS

A Thesis Submitted to
the Graduate School
Izmir Institute of Technology
in Partial Fulfillment of Requirement for Degree

MASTER OF SCIENCE

in Physics

by

Bengü ATA

December 2020

IZMIR

ACKOWLEDGMENTS

I would like to express my sincere gratitude to my supervisor Prof. Dr. Lutfi ÖZYÜZER for his patience and guidance over the past three years during my master thesis. I am thankful for his experience in terahertz region, his ideas to make my master experience productive. I also would like to thank Prof. Dr. Gülnur Aygun ÖZYÜZER for her encouragement and fruitful conversations. It was a great experience to work with ÖZYÜZER research group and perform the experiment in laboratories with the team.

I would like to thank thesis committee members Asst. Prof. Dr. Özge SAĞLAM and Asst. Prof. Dr. Evren ATAMAN for their interest, sincerity and valuable comments.

I wish to thank IYTE TAM specialists for SEM and XRD measurements.

I would also to thank the TÜBİTAK 119R038 project that supported me throughout my work.

I am grateful OZYUZER research group especially my group members Zemzem UYANIK, Alieen NOORI and Yesim ALDURAN. I am also so grateful Dr. Hasan KÖSEOĞLU for his valuable advices and sharing his knowledge generously.

Finally, but not least I would like to thank my family for their patience, support and endless love in all my life's moments.

ABSTRACT

THE GROWTH OF VANADIUM DIOXIDE THIN FILMS BY MAGNETRON SPUTTERING TECHNIQUE AND TERAHERTZ WAVE MODULATION CHARACTERISTICS

Vanadium dioxide (VO_2) is a fascinating material thanks to its unique insulator metal transition (IMT) at 68 $^{\circ}$C which is very close to the room temperature. This reversible change in electrical resistivity is around several orders of magnitude and the electrical change accompanied by optical and structural change as well. Thanks to these unique properties vanadium dioxide material has been studied intensively past decades. This phase transition allows us to apply the transition properties widen application such as field effect transistor (FET), uncooled bolometers, tunable metamaterial filters, high data rate wireless communication etc. Especially for terahertz region which is the most unexplored region of the electromagnetic spectrum, vanadium dioxide is a promising material having ability to modulate terahertz waves by IMT phenomena. In this work, vanadium dioxide (VO_2) thin films fabricated by reactive DC magnetron sputtering method and its properties optimized to minimize the amounts of secondary phases by optimizing the oxygen concentration, sputtering power and deposition time. Samples which show the maximum resistivity change during the transition have been used for the terahertz modulation experiments. It has been observed that when the VO_2 samples triggered by continuous wave (CW) laser, VO_2 transforms to the metallic phase, behave as an opaque material to the terahertz wave. At room temperature, in insulating phase it is partially transparent to terahertz radiation. These results indicate that VO_2 thin films can be a good candidate for THz wave modulators.

ÖZET

MIKNATISSAL SAÇTIRMA YÖNTEMİ İLE VANADYUM DİOKSİT İNCE FİLM BÜYÜTÜLMESİ VE TERAHERTZ DALGA MODÜLASYON KARAKTERİSTİKLERİ

Vanadyum dioksit (VO_2) oda sıcaklığına cok yakın gerçekleşen (68 $^{\circ}$C) yalıtkan-metal geçiş özelliğiyle benzersiz bir malzemedir. Elektriksel direncindeki değişim 10^5 mertebesinde olmaktadır ve bu değişime optiksel ve yapısal değişim eşlik etmektedir. Bu benzersiz geçiş özellikleri sayesinde VO_2 son yıllarda yoğun olarak çalışılmıştır. Bu faz geçişi, vanadium dioksiti alan etkili transistörler (FET), soğutulmamış bolometreler, ayarlanabilir terahertz filtreleri, yüksek veri hızlı kablosuz haberleşme gibi çeşitli alanlarda uygulama imkanı sunar. Özellikle elektromanyetik spektrumun en keşfedilmemiş bölgesi olan terahertz bölgesi için vanadium dioksit, terahertz dalgalarını elektriksel geçiş özelliği sayesinde module etme kabiliyetine sahip umut verici bir malzemedir. Bu çalışmada, vanadium dioksit (VO_2) ince filmleri reaktif DC mıknatıssal saçtırma methodu ile büyütülmüştür ve ikincil fazları minimize etmek için saçtırma gücü, oksijen konsantrasyonu ve büyütme süresi optimize edilmiştir. Yalıtkan- metal geçişi sırasında maksimum direnç değişimi gösteren numuneler terahertz dalgaları modülasyon deneyleri için kullanılmıştır. Sürekli dalga lazeri ile tetiklenerek metalik faza geçmiş numunelerin terahertz dalgalarına karşı opak malzeme gibi davrandığı, oda sıcaklığında yalıtkan fazda olduğunda ise terahertz dalgalarını geçirdiği gözlemlenmiştir. Bu sonuçlar, VO_2 ince filmlerin terahertz dalga modülatörleri olarak kullanılabileceğini göstermiştir.

TABLE OF CONTENTS

LIST OF FIGURES vii

LIST OF TABLES x

CHAPTER 1. INTRODUCTION 1

1.1. Introduction and Motivation 1

1.2. Vanadium Dioxide (VO_2) 2

1.2.1. İnsulator - Metal Transition (IMT) in VO_2 3

1.2.2. Mechanism behind the IMT 7

1.2.3. Parameters Affecting the IMT 9

1.3. Application of Vanadium dioxide (VO_2) 10

1.3.1. Thermochromic Smart Windows 10

1.3.2. Fied Effect Transistor (FET) 11

1.3.3. Tunable Terahertz Modulators 12

1.4. Terahertz Region 14

CHAPTER 2. EXPERIMENTAL 16

2.1. Thin Film Growth 16

2.2. Magnetron Sputtering 17

2.2.1. Experimental 18

2.3. Characterization Techniques 20

2.3.1. X-Ray Diffraction (XRD 20

2.3.2. Raman Spectroscopy 21

2.3.3. Scanning Electron Microscope (SEM) 22

2.3.4. Terahertz Characterization…….. 24

CHAPTER 3. RESULTS 26

3.1. SEM Results 26

3.2. XRD results 27

3.3. RAMAN Analysis.....30

3.4. Electrical Characterization.....31

3.5. THz Characterization 38

CHAPTER 4. CONCLUSION 45

REFERENCES 46

LIST OF FIGURES

Figure **Page**

Figure 1.1. Conductivity as a function of reciprocal temperature for the lower oxides of titanium and vanadium (F.Morin 1959)…….2
Figure 1.2. The optical transmittance of 80 nm VO_2 thin film between the temperatures 25 °C and 100 °C (Kakiuchida et al. 2007)…….....3
Figure 1.3. Change in crystal structure of VO2 during insulator-metal transition (IMT) (Oak Ridge Laboratory 2011)…….....4
Figure 1.4. IMT triggering methods in VO_2 a) Optically triggered (Wu and Liou 2011) b) thermally triggered (Yuce et al. 2017) c) Strain effects on IMT in VO_2 (Chao et al. 2009) d) electrically triggered (Leroy et al. 2012)…….....6
Figure 1.5. a) The band structures of VO_2 in (left) semiconducting phase b) in metallic phase (Goodenough 1971)…….....8
Figure 1.6. Effect of tungsten co-doping on transition temperature of VO_2 thin Films (Soltani et al. 2004)…….....9
Figure 1.7. TEM images of vanadium dioxide precipitates in silicon (left) and their optical transmission as a function of time at wavelength 1.5 µm (right) (Donev 2008)…….....10
Figure 1.8. Working principles of vanadium dioxide thermochromic windows……11
Figure 1.9. Illustration of VO_2 based field effect transistor (FET) (Kim et al. 2004)…….....12
Figure 1.10. a) Hybrid terahertz metamaterial unit cell b) Transmission spectra of Thz metamaterial at 100 °C when the VO_2 in metallic phase and at 20°C when the VO_2 in semiconducting phase (Crunteanu et al. 2012)……13
Figure 1.11. The electromagnetic spectrum (SURA 2006)…….....14
Figure 2.1. Illustration of reactive magnetron sputtering system……..18
Figure 2.2. The picture of a) Magnetron sputtering system b) Growth chamber……..19
Figure 2.3. Geometric derivation of Bragg's Law (Stanjek and Hausler 2004)….....21
Figure 2.4. Energy-level diagrams of Rayleigh scattering, Stokes Raman scattering Anti-Stokes Raman Scattering (Das and Agraval 2011)…….....22

LIST OF FIGURES

Figure **Page**

Figure 2.5. Janis microprobe station in dielectric laboratory…….....23
Figure 2.6. Schematic image of continuous wave THz system…….....25
Figure 2.7. Illustration of sample triggering by CW laser while THz wave pass through…….....25
Figure 3.1. Schematic representation of VO_2 thin films on c-cut sapphire substrate with different thickness and oxygen concentration……..26
Figure 3.2. SEM images a) 2mm b) 5mm of 210 nm VO_2 with 1.36 % oxygen c) and d) 280 nm VO_2 with 1.60 % oxygen concentration…….....27
Figure 3.3. Cross-sectional image of VO_2 film a) 280 nm with 1.60 % oxygen concentration b) 210 nm with 1.36 % oxygen concentration…….....27
Figure 3.4. X-ray diffraction pattern of 280 nm VO_2 thin film with 1.60 % oxygen concentration…….....29
Figure 3.5. X-ray diffraction pattern of 210 nm VO_2 thin film with 1.36 % oxygen concentration…….....30
Figure 3.6. Raman spectra of grown VO_2 thin films with thickness of 210 nm with 1.36 % oxygen concentration and 280 nm VO_2 with 1.60 % oxygen concentration…….....31
Figure 3.7. The resistivity depends on the temperature for vanadium dioxide sample with 1.60 % oxygen concentration……..32
Figure 3.8. The resistivity depends on the temperature for vanadium dioxide sample with 1.36 % oxygen concentration……..33
Figure 3.9. The resistivity depends on the temperature for vanadium dioxide sample with 1.89 % oxygen concentration……..34
Figure 3.10. Electrical behavior of vanadium dioxides (VO_2) thin film samples with different oxygen concentrations…….35
Figure 3.11. Comparison of electrical properties between freshly deposited and one year air exposed VO_2 thin film grown with 2.60 % oxygen concentration……..36

LIST OF FIGURES

Figure **Page**

Figure 3.12. Comparison of electrical properties between freshly deposited and one year air exposed VO_2 thin film grown with 2.40 % oxygen concentration…….....37

Figure 3.13. Full spectrum graph of a) **air** b) **c-cut sapphire (Al_2O_3) +air** substrate at 20 °C…….....38

Figure 3.14. Full spectrum graph of 280 nm **VO_2** + **Al_2O_3** grown with 70W sputtering power, %1.60 oxygen concentration……38

Figure 3.15. Full spectrum graph of 280 nm **VO_2** grown with 70W sputtering power 1.60%……...39

Figure 3.16. THz modulation characteristic 280 nm VO_2 with 70W sputtering power 1.60 % oxygen concentration……...39

Figure 3.17. Full spectrum graph of **VO_2+Al_2O_3** grown with 70W sputtering power 1.89 % oxygen concentration with sapphire……40

Figure 3.18. Full spectrum graph of **VO_2** grown with 70W sputtering power 1.89 % oxygen concentration, 60 minutes deposition time without sapphire substrate…….....41

Figure 3.19. THz modulation characteristic of VO_2 with 70W sputtering power 1.89 % oxygen concentration…….....42

Figure 3.20. Full spectrum graph of **VO_2+Al_2O_3** grown with 50W sputtering power 1.36 % oxygen concentration, 50 minutes deposition time with sapphire…….....43

Figure 3.21. Full spectrum graph of **VO_2** grown with 50W sputtering power 1.36 % oxygen concentration, 50 minutes deposition time without sapphire……..43

Figure 3.22. THz modulation characteristic of VO_2 with 50W sputtering power, 1.36 % oxygen concentration…….....44

LIST OF TABLES

Table **Page**

Table 1.1. Specifications about 1 THz frequency……...10

Table 2.1. Fixed deposition parameters for all vanadium dioxide sample ……....20

Table 3.1. Deposition parameters of VO_2 sample where electrical behaviour shown in figure 3.7……32

Table 3.2. Deposition parameters of VO_2 sample where electrical behaviour shown in figure 3.8……33

Table 3.3. Deposition parameters of VO_2 sample where electrical behaviour shown in figure 3.9……....34

CHAPTER 1

INTRODUCTION

1.1 Introduction and Motivation

Vanadium dioxide (VO_2) is one of the most fascinating strongly correlated electron materials. It has been a focus of research due to its well-known insulator-metal transition accompanied by a structural phase transition since F. Morin discovered the material in 1959. Recent years many exciting discoveries occur about both understanding of physics of vanadium dioxide and also developments of the new application of VO_2-based materials. This is thanks to new synthesis methods, computational power and new developments in scientific instrumentation allow us new discoveries. VO_2 has become most extensively studied correlated metal oxide since the transition occurs very close to the room temperature. While transition temperature for Nobium dioxide (NbO_2) is 807 $^{\circ}$C this value drops to 68 $^{\circ}$C for vanadium dioxide (VO_2) (Gervais and Kress 1985). This relatively low phase transition enables us to work on the transition characteristics for widen applications such as ultrafast optical switching, metamaterials, thermochromic smart windows, uncooled bolometers, thermal actuators, field effect transistors, tunable THz filters and so on.

It has been great effort given to filling the so-called THz gap in the past decade and by new generation of metamaterials which respond to THz region making this gap accessible. Terahertz waves have been investigated in recent years owing to the benefits of bandwidth and photon energy (Ferguson et al. 2002). There have been given great effort in high-performance THz devices for the improvement of component minimalization (Nouman et al. 2016; Barani et al. 2020). THz modulators are important in THz technology as they are key elements for applications such as wireless communication, imaging and sensitive thermal dedectors (Namai et al. 2009; Landy et al. 2009; Zhang et al. 2019). It is crucial to have tunable modulators. In order to make active THz modulators, suitable materials with tunable optical features are vital. From this aspect VO_2 is a perfect candidate as a modulation element since by using insulator-metal transition phenomena with external sitmuli these modulators can be active and passive.

1.2. Vanadium Dioxide (VO_2)

Vanadium oxides (VO_2) are quite complicated. A small change in temperature, applied voltage, % oxygen, effecting the morphologies, phases and states of the material. Vanadium has several valence states (+2, +3, +4, and +5) in oxides, which makes it challenging the growth of a pure phase vanadium dioxide thin films. This multiple valence states leads to great variety of compounds such as VO, V_2O_3, V_4O_7, V_5V_9, V_6V_{11}, V_7O_{13}, V_8O_{15}, VO_2, V_2O_5 etc. However, the insulator-metal transition (IMT) temperature is close to the room temperature only for vanadium dioxide (VO_2). 1959 Morin showed the resistivity change around critical temperature for the oxides of vanadium and titanium (Fig. 1.1). VO_2 with V_2O_3 and VO showed IMT characteristics.

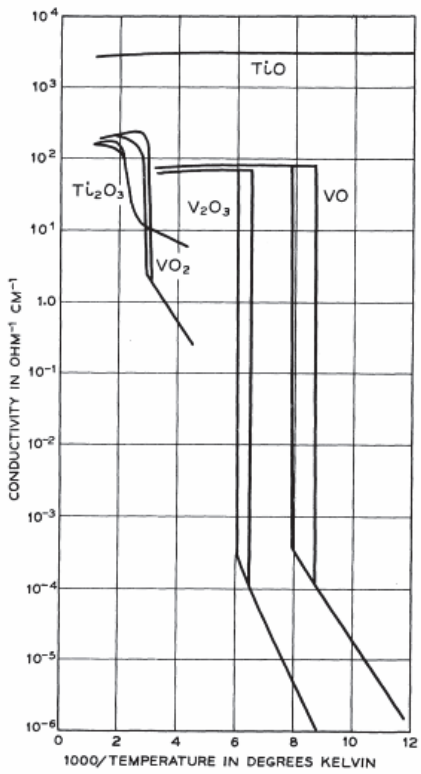

Figure 1.1. Conductivity as a function of reciprocal temperature for the lower oxides of titanium and vanadium described (Source: F. Morin 1959).

The IMT in VO and V_2O_3 showing the resistance change above five orders of magnitude. The transition temperature for VO_2 is above room temperature. On the other hand, VO and V_2O_3 shows the transition temperature $T_c$vo = 120K and T_cv2o3 = 159K respectively. This distinctive feature of VO_2 makes this material very intriguing for optical and electronic devices which needs switching.

1.2.1. Insulator-Metal Transition in VO_2

VO_2 is a promising material thanks to its insulator–metal transition (IMT) phenomena with outstanding changes in its optical, electrical and structural properties at temperatures around 68 °C. VO_2 has taken lots of attention owing to having this transition temperature being close to room temperature. VO_2 is a transition-metal oxide and considered to be a n-type insulator below the T_c . It undergoes a first-order phase transformation at the critical temperature T_{IMT} of ~68 °C and presents an insulator state with a monoclinic structure below $T_{IMT,}$ but behaves as metal with a tetragonal rutile structure above T_{IMT} (Imada et al 1998) . This transition not only change electrical properties but optical properties as well.

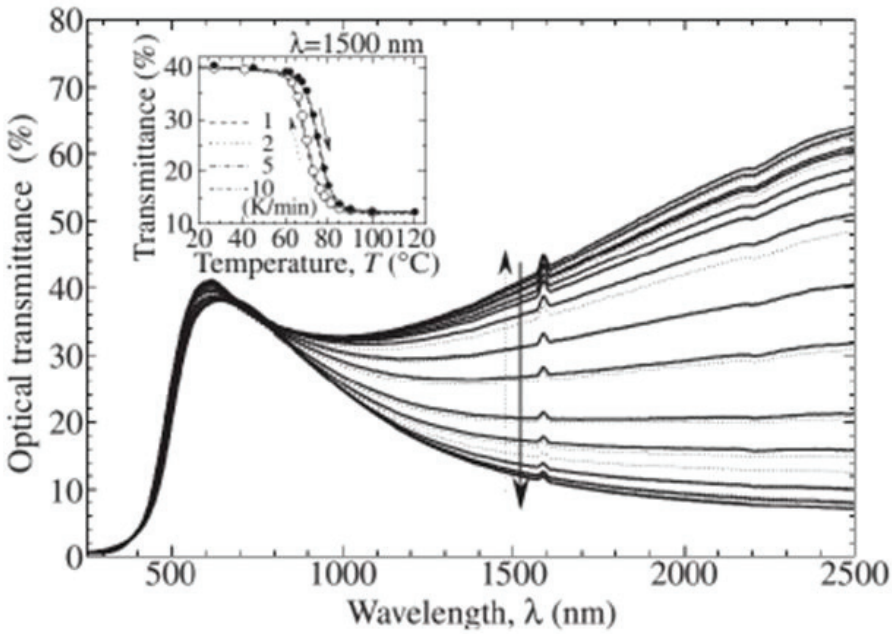

Figure 1.2. The optical transmittance of a VO_2 thin film of 80 nm for temperatures between 25 °C and 120 °C (Source: Kakiuchida et al. 2007).

An example is shown in figure 1.2 optical transmittance spectra of 80 nm VO_2 thin film grown on silicon at temperatures around IMT transition. Below T_c, VO_2 which in monoclinic phase, with an energy gap of 0.65 eV, allowing high IR transmission (Yi et al. 2003; Chang et al. 2018). Above T_c, VO_2 is in the metallic phase, in which overlap between the Fermi level and the V *3d* band eliminates the band gap, causing the material to be highly reflective or opaque in the near-infrared region. What is more, the critical temperature can be decreased to near-room temperature.

A structural transition accompanied by electrical transition simultaneously. The insulator low-temperature structure is monoclinic and called as the VO_2 (M1) phase. At high temperature the lattice transforms to a body-centered tetragonal rutile structure called as VO_2 (R). Both of the structures are shown in figure 1.3 where red color represents oxygen atoms and blue color vanadium atoms.

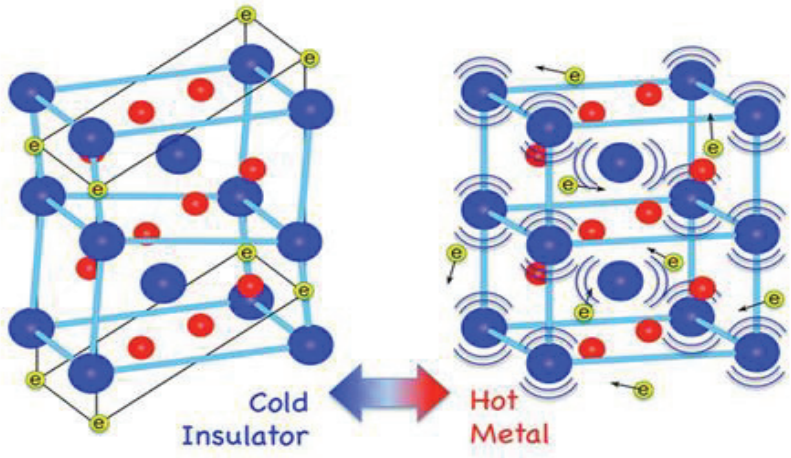

Figure 1.3. Change in crystal structure of VO_2 during the IMT
(Source: Oak Ridge Laboratory 2015).

In the M1 phase, vanadium atoms form a zigzag shape along the c-axis. The short and long V-V bonds are 2.619 and 3.164 Å. In this phase, the d bands are pushed toward the valance band which makes the material insulator. Above the T_c, in metallic phase, the crystal structure expands to a tetragonal rutile structure with removal of the zigzag V chains allow the occupation of cunduction band by electrons. The length of V-V along the c-axis gains a constant value of 2.815 Å. There are other intermadiate phases of VO_2

as well. Additionally to M1 and R phases other insulating phases has been observed like M2 phase, the M3 phase, and also triclinic T phase too. Among them, the M2 phase has been investigated intensively due to fact that having similar dielectric properties but different magnetic properties with the monoclinic phase. Within the M1 phase, both the metal–metal pairing and therefore the zigzag type lateral displacement are observed on each chain, but in the intermediate M2 phase, only 1/2 the chains dimerize and therefore the zigzag-type irregularities are restrained to the opposite 1/2 the chains. These new guest phases bring extreme difficulties for directly investigating the phase transition; but it can be important to understand the mechanism of the IMT if these phases could be examined independently. Moreover, in M2 phase the V4+ ions form equally spaced V chains, and experiments indicate that they act magnetically as S = 1/2 Heisenberg chains (J = 300 K). It's obvious that the V–V chain in M2 phase are magnetic insulators. Indeed, LDA calculations for the M2 phase causes anti ferromagnetic state almost like the monoclinic insulator phase, this failing can be solved by LDA+U approximations.

Temperature is considered to be the main parameter that triggers the IMT but also it can be triggered by electrical, optical and pressure-induced method too as shown in Fig 1.4 (Yang et al. 2011). The IMT take place quite fast, around 80 fs and experimentally proven by optical pump-probe methods (Cavalleri et al. 2004).

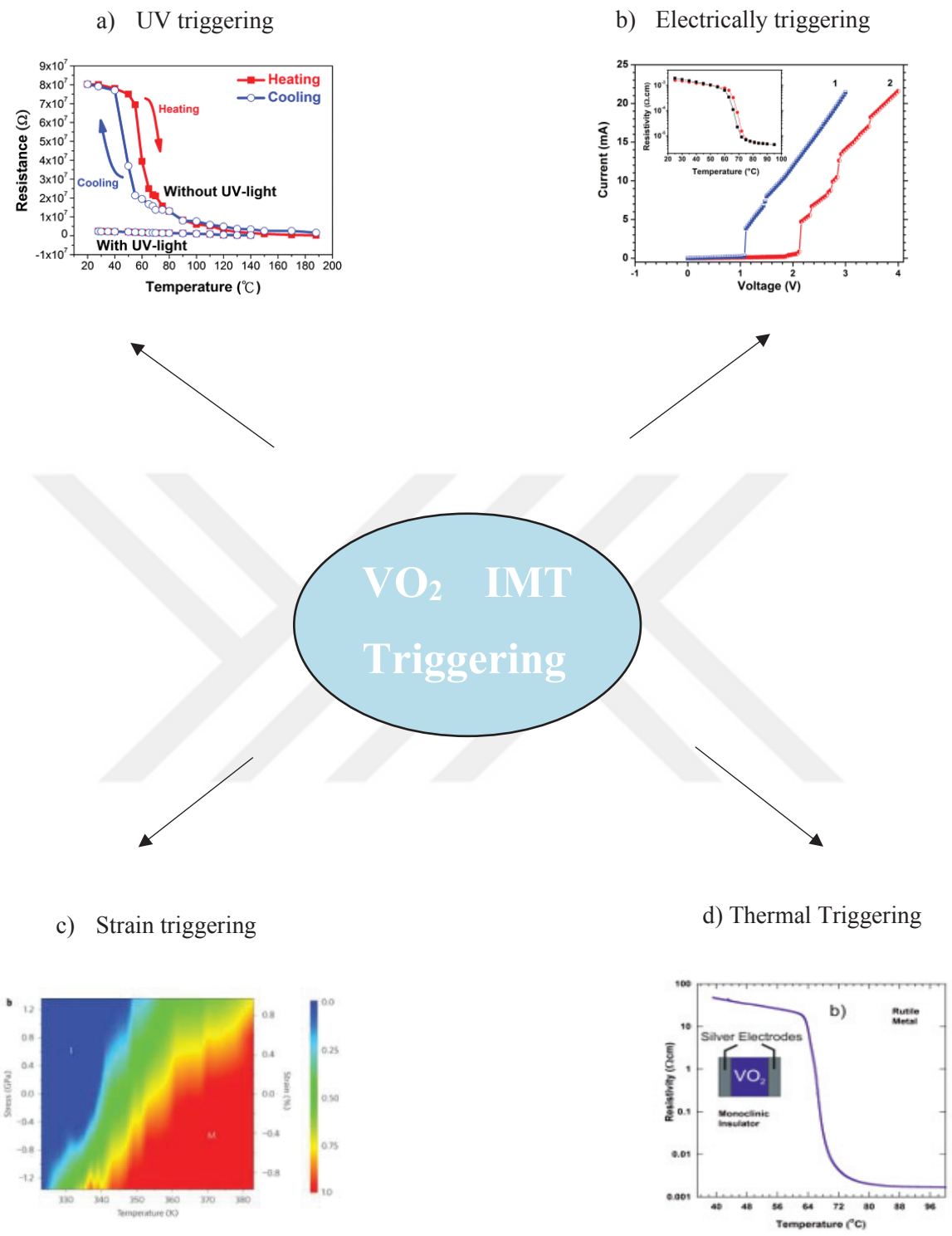

Figure 1.4. IMT-triggering methods in VO_2. (a) Optically triggered (M. Wu and B. Liou 2011) (b) Electrically triggered IMT (J. Leroy et al. 2012). (c) Strain effects on IMT in VO_2. (J. Cao et al. 2009) (d) Thermally triggered IMT (Yuce et al. 2017).

As shown in figure above, there is hysteresis loop occur between heating and cooling in resistance versus temperature graphs. There are some parameters which influence the hysteresis width in VO_2. Grain size, grain boundaries, doping, porosity and crystallographic orientation effecting the width. According to experimental results, the hysteresis width of polycrystalline VO_2 thin films, in general is relatively large. It is observed that there is inverse proportion between grain size and hysteresis width. However, well-defined grain boundaries causing larger hysteresis width since each grain boundaries undergoes the IMT independently, one after the other. Thin films without distinct grain boundaries, works cooperatively so that narrow hysteresis occurs. The porous thin films contain more structural defects which has a tendency to block the recovery. This is to say, the delay in transition across the cooling phase causes larger hysteresis.

1.2.2. Mechanism behind the IMT

The mechanism of the IMT in VO_2 has been intensively studied. However, a full understanding of transition dynamics remains puzzling. Over the years, the debate over the mechanism guiding the IMT has intensified. Mainly two scenarious are encountiring. One is Peierls approach which try to explain via lattice distortion, the other one is Mott theory which explaning by electron-electron correlation. Since the transition has elements from both Mott and Peierls type mechanisms, recent works have suggested a solution to the argue with an intermediate explanation in terms of "Peierls-Mott" pictures (C. Weber, et al. .2012; Tomzcak et al. 2008; B. Lazarovits et al. 2010).

Classical theory says that the difference between insulator and conductor defining by electronic bands that is result of lattice structure and their occupation by electrons. At zero temperature insulators have fully filled valence band and metals have partially filled valence band enable electrons move through lattice. Semiconductos are having small bandgap between valence band and conduction band. Thermal excitation allows certain degree of freedom for electron between valence band and conduction band.

In 1937 de Boer and evert Warvey showed that many transition-metal oxide even they have partially d-electron band they behave like insulators. This behaviour caused by electron-electron interaction. It is the coloumb interaction between electrons which is responsible electron immobility between unitcells. Mott criation indicates that critical

charge density described by the equation $n^{-1/3} < Ca_0^*$ where a_0^* is effective Bohr Radius. Transition takes place when critical charge density increases which is due to higher lattice constant (Mott 1990).

Because of the structural change in the crystal during the electronic transition, Mott's correlated electron theory cannot explain this phenomena totally. Peierls electron-phonon theory come up with an alternative mechanism which try to explain this transition. The periodic potential causes a change in band structure which triggered by structural deformation. Goodenough described the both structures of VO_2 at temperatures below and above T_c and it is shown in figure 1.5. In metallic phase the conduction bands is partially filled.

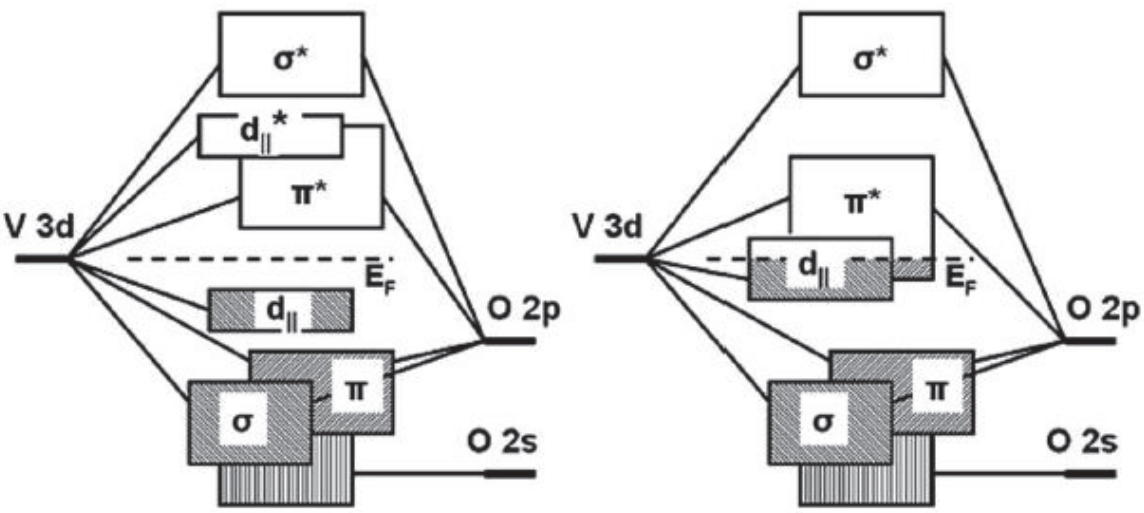

Figure 1.5. The band structure of VO_2 in (left) semiconducting phase and (right) metallic phase (Source: Goodenough 1971).

The origin of IMT is still a subject of debate till now; is it a result of carrier-induced Mott type transition or caused by structural change namely Peierls type transition. One study shows by using local density approximation calculations that instead of Mott insulator, M1 phase that below T_C in insulator phase it should be treated as normal insulator (Wentzcovich et al. 1994). On the other hand because of the existance of

intermediate phases like M_2 structure which is Mott type, transition is much more difficult to explain (Rice et al. 1994). Another study shows that by ultrafast spectroscopy, IMT takes 80 fs which is the half period of lattice vibration (Cavalleri et al. 2005). This result is supporting that it can be possible evidence of Mott type. Recently, DFT calculations show that below T_C vanadium dioxide cannot be considered as pure Mott type insulator, it should be considered as a many-body Peierls insulator. Peierls mechanism and electron-electron interaction should be counted to describe the driving mechanisms of transition.

1.2.3 Parameters affecting the IMT

VO_2 undergoes insulator-metal transition at temperature near 68˚C. During the transition the resisitvity of thin films change by three to five orders of magnitude. Neverthless, in thin films these characteristics are seldom and can be shifted by several parameters like doping, stress, grain size, pressure and and stoichiometry. In the following paragraphs it will be discussed how these paramaters changing transition temperature, transition sharpness, hystheresis width etc.

Doping: For the purpose of changing the transition temperature doping is a frequently used technique. Tungsten, molybdenium and niobium are some elements used to dope vanadium in the literature. By tungsten co-doping transition temperature decreased to 45˚C for VO_2 thin films as shown in figure 1.6 (Soltani et al. 2004).

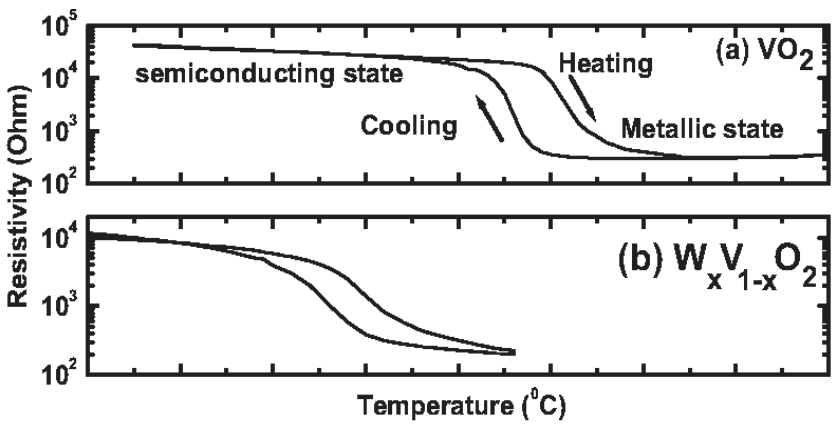

Figure 1.6. Effect of tungsten co-doping on transition temperature of vanadium dioxide films.

Grain size: The grain size of VO_2 influencing the phase transition characteristics, such as the shape of the temperature hysteresis width. The effect of grain size observed in some studies examining the transition in nanoparticles embedded in silicon and sapphire substrate as shown in figure 1.7 (R. Lopez et al 2002).

It has been observed in nanoparticles that hysteresis width increasing by heterogeneous nucleation (Donev 2008). In other words, it can be said that the transition starts at defects. The more driving force of transition increasing, the number of active defects is increasing. It is clear that smaller crystallites are having less defects. This result explains why in nano particles hysteresis width are widen.

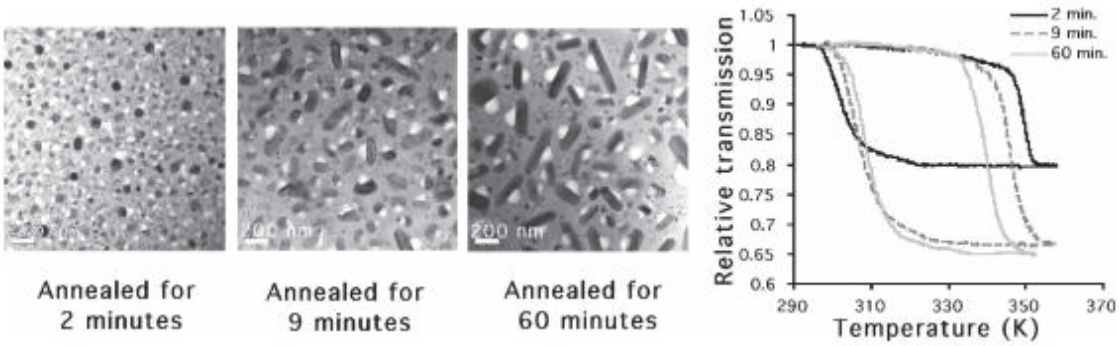

Figure 1.7. TEM images of vanadium dioxide precipitates in silicon substrate (left) and their optical transmission as a function of time at wavelength 1.5mm (right). Showing the decreasing annealing time decreasing the size of nanoparticles cause an increase in hysteresis width.

Stoichiometry: To grow VO_2 thin films in single crystal form with controlled oxygen stoichiometry is one of the most challenging tasks, especially in the case of transitional metal oxide thin films, where ions are having many possible oxidation states. The effect of stoichiometry on IMT in vanadium dioxide has been studied (Griffiths and Eastwood 1974). It has been observed a decrease in transition temperature in oxygen lacking thin films.

1.3. Applications of Vanadium Dioxide

1.3.1. Thermochromic Smart Windows

Applications of thermochromic smart windows by using vanadium dioxide thin films are popular thanks to the optical transmission change during the IMT. The principle is shown in figure 1.8. As VO_2 undergoes reversible transition from insulator to metal, the amount of transmitted solar radiation is decreasing. In metallic phase, it is opaque to infrared radiation and transparent to infrared in semiconducting phase. By this way in the winter IMT coating on glass will let more light pass through the window and in the summer the situation will be reserved that most light will be reflected make the building cooler. Owing to this unique transition property makes vanadium dioxide thin films a promising material for smart windows.

Reducing the IMT temperature plays an important role for commercial use. As mentioned previous section by doping the VO_2 thin films like tungsten this target can achievable. Yellowish color of thin film coatings makes VO_2 less attractive for commercial use. By doping the VO_2 nanoparticles with Mg or F gives us a solution to overcome this issue (Soltani and Kaye 2015).

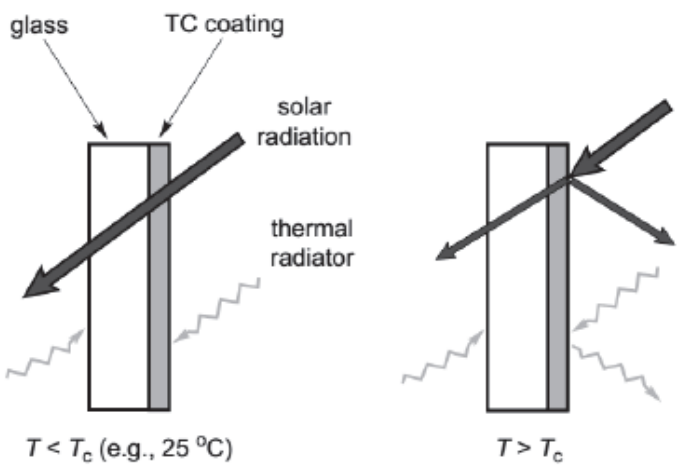

Figure 1.8. Working principle of vanadium dioxide thermochromic window

1.3.2. Field Effect Transistor

Field effect transistor (FET) is another device using again the IMT characteristics of VO_2 thin films. Basic working principle is that by applying the voltage on the gate electrode changing the resistance of the gate channel which connects to source and drain. In metallic phase correspond to low resistance channel is on state and in semiconducting phase corresponds to high resistance it is off state. In figure 1.9 VO_2 based field effect transistor is shown.

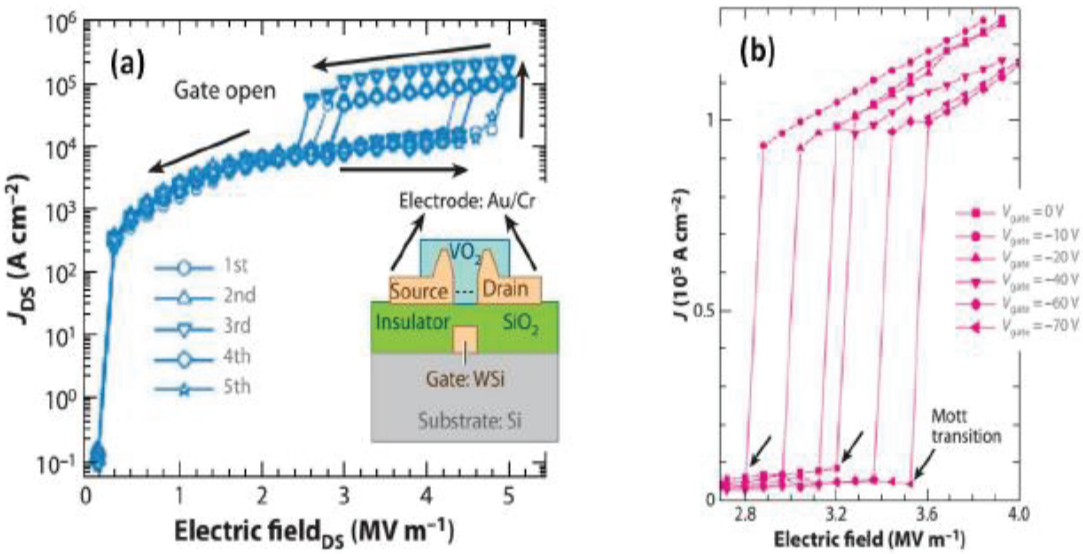

Figure 1.9. Illustration of VO_2 based FET
(Source: Kim et al. 2004).

1.3.3. Terahertz Modulator

Terahertz waves locate in an important frequency range in the electromagnetic spectrum since it carries crucial information which has possibility to be used in cutting-edge technologies like signal detection, wireless communication, security imagining etc. Particularly THz wave can address the high demand of ultra-high speed wireless communication. In most communications systems, the maximum carrier frequency is 60 GHz and the bit rate is around 1 Gbps. In order to reach big-volume data transfer, frequency should be above 100 GHz which is lying in THz region. The progression of THz technology depends on the improvement of efficient components like filters,

switchable mirrors, dynamic polarization controllers and phase modulators. For this purpose, active and rapid manipulation of THz wave propagation is needed. Consequently, Terahertz modulators became crucial device in Terahertz communication systems. There are different modulation techniques for the manipulation of the electromagnetic properties of waves in terahertz regime. Frequency shift, phase and amplitude are some physical quantities that are manipulated by modulators. By this way the modulator imprints the specific reflection or transmission characteristics onto terahertz wave. One way of terahertz modulation is tuning the electrical conductivity of the material so that a change occur in the transmittance and reflectivity of the terahertz wave transmits in the material. VO_2 which having insulator-metal phase transition with accompanying high transmittance in insulator phase and opposite property in metallic phase make this transition- metal oxide thin film a promising candidate as a THz modulator. When there is an external stimuli like laser or thermal source which trigger the IMT in VO_2, thin film behaves as a metal hence incident THz wave cannot transmit through the VO_2, in insulator phase, below the critical temperature thin film is transparent to the THz waves so that THz wave transmit through the VO_2 thin film . It is quite practical way of THz modulation. One way for THz wave manipulation is to design artificial constructed surfaces which is called meta-surfaces. By designing various materials with desired structure, they gain ability to manipulate THz radiation. In figure 1.10 shows the changing transmission response of a tunable metamaterial based on the vanadium dioxide as VO_2 undergoes from insulator to metallic phase.

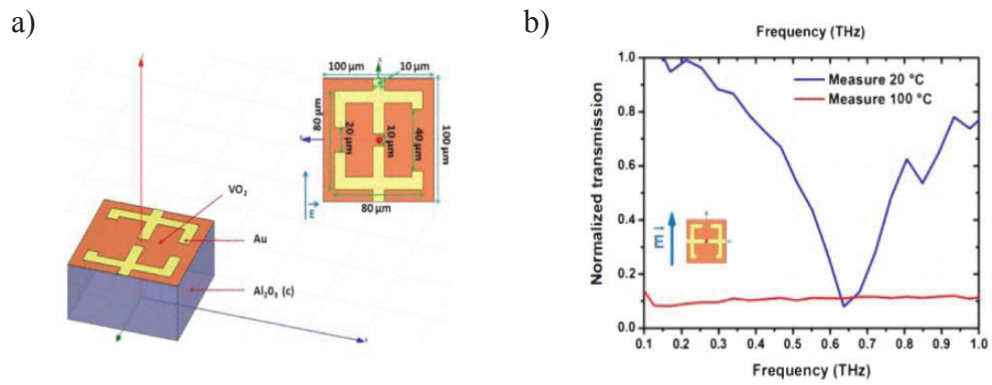

Figure 1.10. a) Hybrid terahertz metamaterial unit cell b) Transmission spectra of THz metamaterial at 100 °C when the VO_2 in metallic phase and at 20 °C when the VO_2 in insulator phase (Crunteanu et al. 2012).

1.4 Terahertz Radiation

Terahertz (THz) radiation is the least explored and used region of the electromagnetic spectrum which lies between the boundaries of electronics and photonics. In the wavelength domain it is from 3mm to 30 μm between microwave andfarinfrared with the correspond frequency from 100 GHz to 10 THz (Gopalan and Rodriguez 2019).

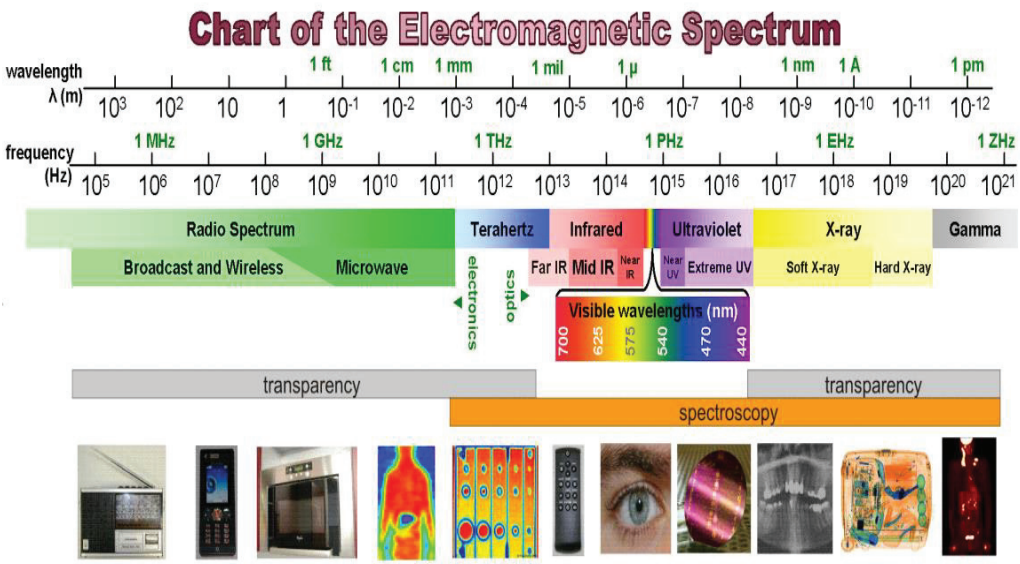

Figure 1.11. The Electromagnetic spectrum
(Source: SURA 2006).

In order to examine Terahertz region better, characteristics about 1 THz is given below table 1.1

Table 1.1. 1 Terahertz specifications.

For 1 THz Frequency	
Temperature	48 K
Wavelength	300 μm
Wavenumber	33 cm^{-1}
Photon energy	4.135 meV
Period	1 ps

Although because of the lack of THz detectors and sources this region called as THz gap, recent improvements in high frequency part of the microwave electronics and low frequency part of photonics research make this gap smaller. With the help of high-power sources (Ozyuzer et al. 2007) and more sensitive dedectors (Alaboz et al. 2017) this gap has been narrowed last decades. There are many reasons why there is a demand for the devices work in THz region. One of the main reasons is that owing to its low photon energy it does not ionize the living organism. This property makes THz region popular in medical research (Ouchi et al. 2014). Another significant property of THz wave is that it passes through the nonpolar and nonconducting materials but absorbed by water vapour. THz wave reflects from metals therefore it can be used to detect hidden guns. THz radiation is also promising candidate for high rate wireless communication. The effect of water absorption on the wave propagation at the infrared and optical region put a barrier in their widen usage for high rate communication. However, THz radiation is less scattered from fog make it better candidate for high rate wireless communication.

CHAPTER 2

EXPERIMENTAL

The essential purpose of this thesis is to growth and characterization of VO_2 thin films on c-cut sapphire [Al_2O_3 (0001)] by reactive DC magnetron technique and investigation of possible terahertz applications. In order to investigate its structural, electrical and optical properties so that the quality of the films, various methods has been applied such as scanning electron microscopy (SEM), Raman spectroscopy, X-Ray diffraction (XRD) and UV spectrophotometry. For the electrical characterization microprobe station under vacuum is been used. For the thin films that achieved resistance difference above 10^3 is been examined for THz characteristics.

2.1. Thin film growth

Thin films are the atomic layers where their thickness changing between from several atomic layers up to micrometers. By coating objects, properties can be improved, or added new features. The constant development of deposition technology is guided by the demand on current deposition technology as well as to change conventional methods with novel techniques. The development in deposition also gives us opportunity for new application areas where the new methods can be performed. Based on the material properties, thin film deposition techniques can be divided into two main category as chemical vapor deposition (CVD) or physical vapor deposition (PVD). In CVD, for the deposition of desired material, with or without carrier gas, chemical vapor breakdown on the substrate. Physical vapor deposition processes based on the transformation of desired material which is called target from condensed phase to vapor phase in vacuum and then condense the vapor on substrate for coating.

There is plenty of thin film deposition techniques such as pulsed laser deposition (PLD), atomic layer deposition, molecular beam epitaxy (MBE), magnetron sputtering, chemical vapor deposition (CVD), spray pyrolysis, thermal oxidation and sol-gel methods that has been used to synthesis vanadium dioxide thin films. Magnetron sputtering which

is the dominant method of physically deposition films by plasma method is most suitable technique for VO_2 due to having large are growth, low cost, high purity, uniformity and high crystal quality attract us to choose this technique for fabrication.

2.2. Magnetron sputtering technique

Magnetron sputtering is physical vapor deposition (PVD) method. The target is sputtered by Ar ions resulting of ejection of ionic and atomic features from target material. Fig 2.1 shows the basic diagram of reactive DC magnetron sputtering system. Sputtering system consist of electrodes namely cathode and anode which is apart from several cm from each other and optimized distance been applied for best results. The substrate positioned on the anode and the target material is on the cathode. Argon / oxygen gas mixture is sent into chamber and then certain direct current voltage is applied to the electrodes in order to make argon atoms ionized so that plasma discharge starts. Magnetic field created by the magnets under the target. The purpose of creation of magnetic field is to trap electrons close to the target so that at lower pressures ionization can start. For VO_2 deposition, the positive particles from the plasma are accelerated by the electric filed between anode and cathode and then argon ions hit the vanadium atoms out of target. Between the sputtered vanadium atoms and the oxygen on the heated substrate chemical reaction occur to form VO_x films. Sputtering process is controlled by DC (direct current) power. It is noted that for targets that made of nonconducting materials radio frequency (RF) power should be applied to between anode and cathode to achieve sputtering process otherwise no plasma occurs.

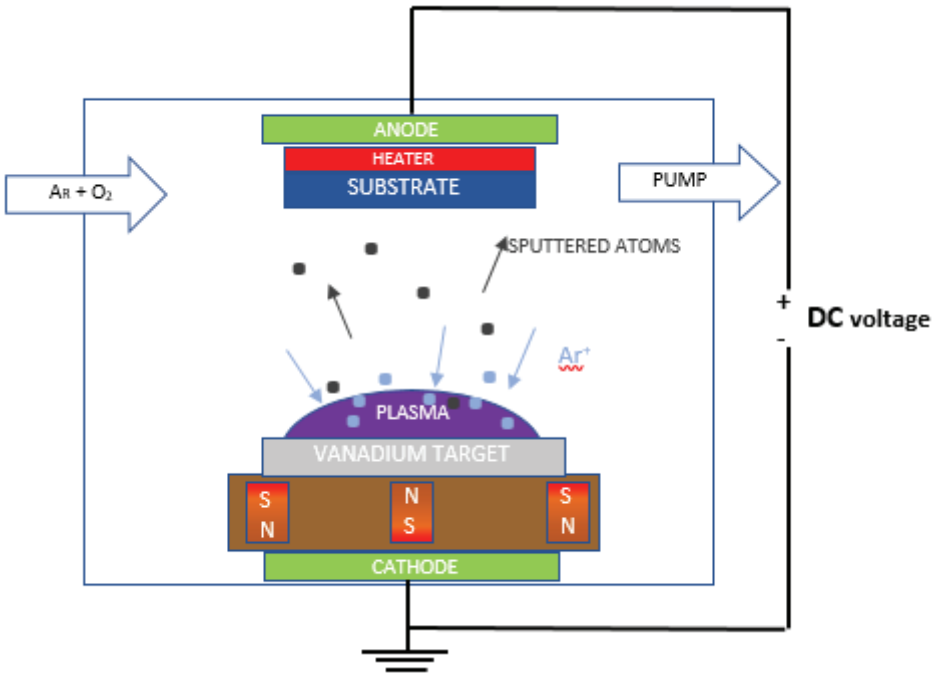

Figure 2.1. Illustration of reactive magnetron sputtering system.

2.2.1. Experimental details

For VO_2 thin film deposition c-cut sapphire (Al_2O_3) was used thanks to its good thermal conductivity 27.21 Wm^{-1} K^{-1} at 300 K. The sapphire substrate was cleaned in the order of acetone, methanol and propanol in ultrasonic vibration for 10 minutes each step. The pure nitrogen gas was used to dry up the substrate. After that, placed the substrate on the holder. Chamber is evacuated to $3.0x10^{-6}$ Torr base pressure before heating up the substrate. Heater was designed to heat up the substrate shown in figure 2.2. As a heater source 4 lamps with the power 250 watt was used and controlled by PID controller connected to J-type thermocouple. After opening up the heater, in order preserve the vacuum level, each 10 minutes the power of the heater increased by 10 % till the reaching up to 550 $^{\circ}$C. In order to get rid of contamination on the target surface, presputter with 50 sccm argon gas was performed for 10 minutes before the deposition. After 10 minutes presputtering, for the purpose of getting VO_2 thin film, in Ar + O_2 mixed environment, deposition was performed with constant DC sputtering power at 550 ^{0}C. High purity (99.95%) vanadium target was used for the deposition. For the uniformity of the deposited thin films and dissipation of the heat on the substrate homogeneously, substrate holder was connected to a DC motor with the rotation power of 15 rpm.

a) b)

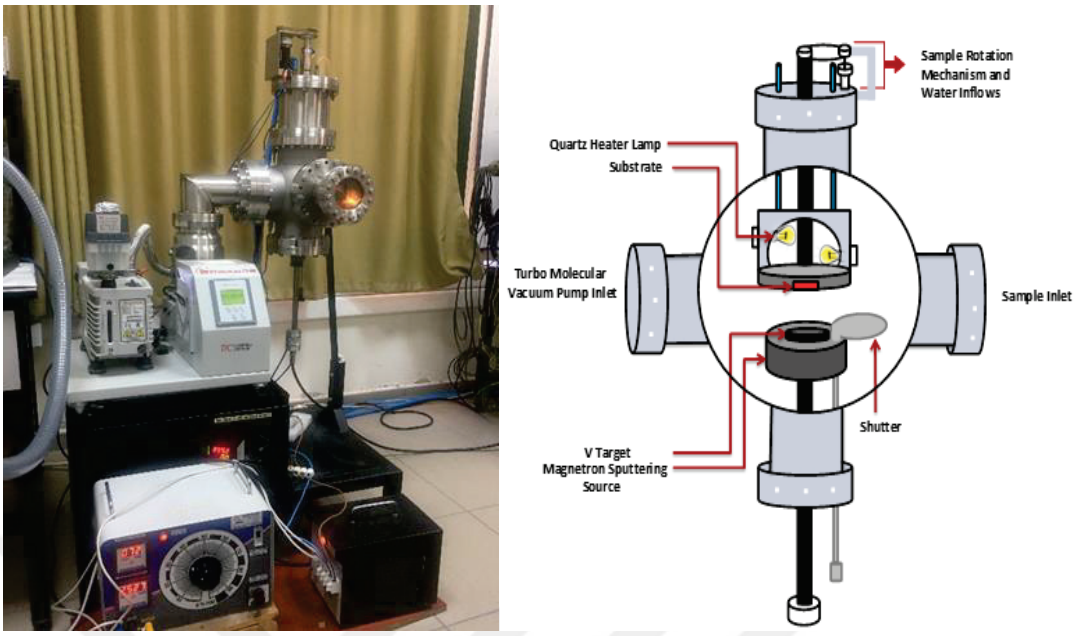

Figure 2.2. The picture of a) DC Magnetron sputtering system b) Growth chamber

After the deposition, in order to enhance crystallinity of the thin films, heating power decreased 10 % of power each 10 minutes. Since vanadium dioxides are very sensitive to oxygen concentration and thickness so that deposition time, in order to obtain vanadium dioxide phase, and minimize the secondary phases, different oxygen concentration and deposition time were applied for optimization. The parameters which kept constant during deposition are shown below table 2.1.

Table 2.1. Fixed Deposition Parameters for all Vanadium Dioxide Thin Films.

Deposition conditions	Value
Substrate Temperature	550 °C
Argon flow	136 sccm
DC sputter power	70 watt
Base pressure	$3x10^{-6}$ Torr
Operating pressure	$5x10^{-3}$ Torr

2.3. Characterization Techniques

2.3.1. X-Ray Diffraction

X-Ray diffraction (XRD) is used to characterize both polycrystalline and epitaxial thin films. XRD is a powerful non-destructive technique for material phase characterization and useful tool to investigate the crystal structure, grain size, strain etc. The basic working principle of XRD system is simple actually. X-rays are electromagnetic wave that its wavelength is around angstrom which is very close to the size of an atom. The dominant effect is the diffraction, without any diffraction effects, there would be not interference appear, the incidence of a primary X-ray beam onto a target would produce scattering in all directions. Thanks to the lattice structure which is regular pattern of an atom repeating itself the scattered X-rays cause constructive and destructive interference in a target material due to having regular pattern. X-Ray diffraction defined by Bragg's Law:

$$2d \sin\theta = n\lambda$$

Where d is spacing between the atomic layers of crystal, θ is the angle of incident beam between lattice planes, n is an integer number and λ is the wavelength of the radiation shown in Fig. 2.3.

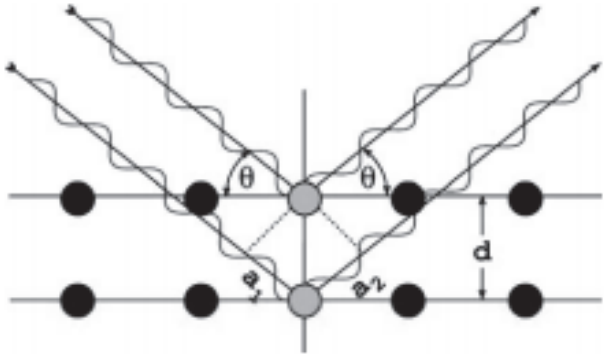

Figure 2.3. Geometric derivation of Bragg's law: Constructive interference occurs when the delay between waves scattered from lattice planes given by a1 + a2 is an integer multiple of the wavelength λ (Source: Stanjek and Hausler 2004).

2.3.2. Raman Spectroscopy

It is an analytical technique that is used to have information about vibrational, rotational and low-frequency phonons in a material, which materialize after the discovery of the Raman effect by Sir C.V. Raman. in 1928. Raman effect, also known as Raman scattering, detects the vibrational modes called phonons in molecule. When photons are scattered form atoms or molecular, most phonons are scattered photons still maintain the same kinetic energy and frequency, and this kind of scattering following into this category is defined as Rayleigh scattering or elastic scattering. (Fig. 2.4). On the other hand, very small amount (~1/107) of the distributed radiation is moved to another wavelength, named "Raman scatter". The majority of these raman scattered photons are moved to greater wavelengths, which is called Stokes shift. Moreover, a few numbers are moved to inferior wavelengths, which is called anti-Stokes shift. Stoke radiation occurs at lower than the Rayleigh radiation energy whereas anti-Stokes energy has bigger energy. The increase or decrease in energy is related to the vibrational energy levels in the ground state of the molecule. The observed Raman shift of the anti-Stokes and Stokes directly measure of the vibrational energies.

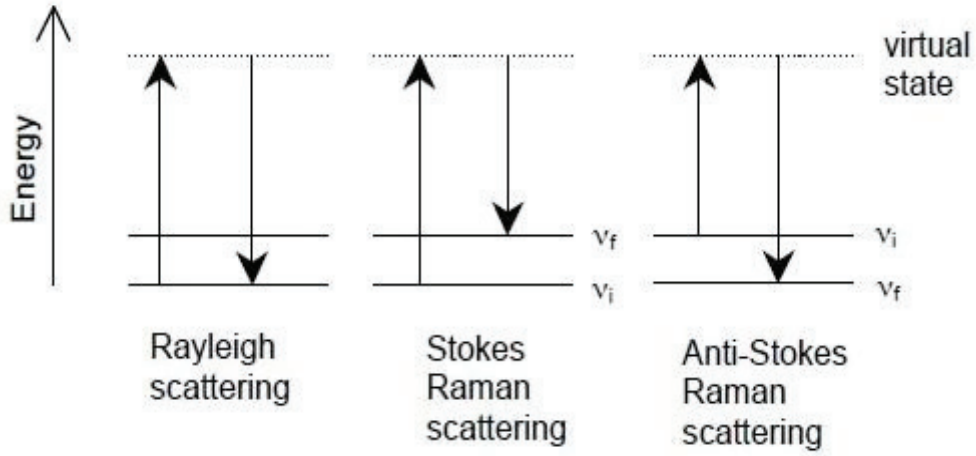

Figure 2.4. Energy-level diagrams of Rayleigh scattering, Stokes Raman scattering and anti-Stokes Raman scattering (Source: Das and Agraval 2011).

Raman analysis was carried out by confocal Raman spectroscopy with an excitation wavelength of 514.5 nm which is located in the Physics Department of IZTECH, and this technique is used to obtained vibration modes of vanadium oxide thin films.

2.3.3. Scanning Electron Microscopy (SEM)

Scanning electron microscopy (SEM) and EDS gives us information about surface morphology, structure, composition and element. Generation of information achieved via secondary electrons, back scattered electrons and characteristics X-ray. Secondary electrons which is a kicked out electron from its shell by an incident electron gives us information about surface morphology. Back scattered electrons are the incident electrons return back from the specimen gives the composition contrast. Characteristic X-rays are generated when outer-shell electron fills the vacancy in lower-shell which is caused by incident electron hits the electron in the shell and they are detected by EDS. This emitted X-rays are characteristics for each atom so it gives us information about the elements in thin films. Generation region of secondary electrons is up to 10 nm, for back scattered electrons is 300 nm and for characteristic X-rays up to 1000 nm and these values depends on surface density and accelerating voltage.

The surface morphology and structure were investigated by scanning electron microscopy which is located at TAM of IZTECH. In addition, thickness of the films measured by SEM- cross sectional image of the sample.

2.3.4. Electrical Characterization

Electrical properties of vanadium oxides thin films were investigated in microprobe station under vacuum shown in Figure 2.4. The resistance values at temperatures between 295 K and 350 K acquired with Keithley 2100 digital multimeter and simultaneously recorded via LabView program. By this way, insulator-metal transition characteristics of the thin films were observed while samples were heated. For the vanadium dioxide thin films which have highest ΔR value were used for THz modulation characterization experiments.

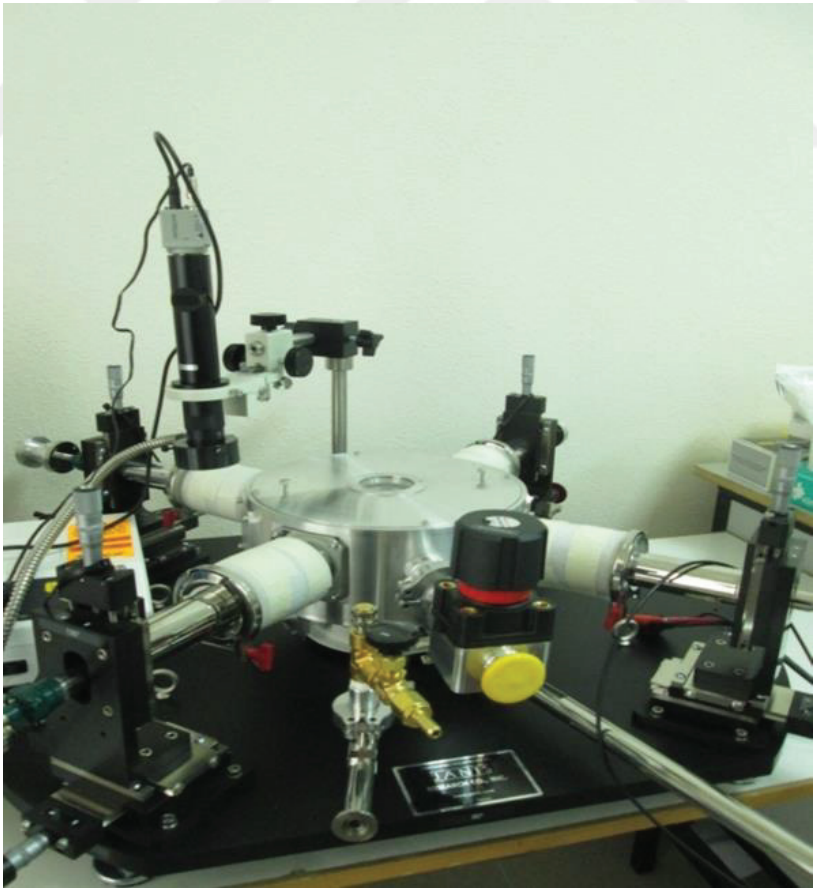

Figure 2.5. Janis Microprobe station in dielectric laboratory.

2.3.5. THz Characterization

The schematic view of the Continuous Wave Terahertz (THz) system is shown in Figure 3.1. CW THz system consist of the THz Source operating in the frequency range 0.500 - 0.750 THz which has a RF Generator, frequency counter and VDI WR1.5 AMC (Amplified / Multiplier Chain (Amplified / Multiplier Chain), 90 ° off axis parabolic mirror (4 pieces) and Golay Cell as a detector.

The THz wave, emitted from WR1.5 AMC, was first modulated by a function generator with 15 Hz frequency and 2.5 V peak to peak voltage using the TTL modulation option of the WR1.5 AMC, and then collimated by a pair of 90° off-axis parabolic mirrors and focused into the sample holder origin. After the interaction of the THz waves and sample the transmitted THz wave was collimated by a second pair of 90° off-axis parabolic mirrors and focused into the Golay Cell. Finally, the collected signals by the Golay Cell were analyzed by a lock-in amplifier. Continuous wave (CW) 915 nm laser is positioned in front of the vanadium dioxide thin films in order to trigger IMT.

In order to obtain the Terahertz transmission spectrum of the samples in the 0.500 to 0.750 Terahertz frequency range, the vanadium dioxide thin films (**background (air)**, **c-cut sapphire**, **deposited thin film**) was fixed to the focal point of the sample holder and then the transmitting Terahertz wave collected by the lock-in amplifier in the 0.500 to 0.750 THz frequency with the 0,0025 Terahertz (2.5 GHz) resolution. After that, THz transmittance (% T_{THz}) of thin films can be calculated by the following formula;

$$\%T_{THz}(\nu) = \frac{(S(\nu) - N(\nu))}{(B(\nu) - N(\nu))}$$

here, S(ν), B(ν) and N(ν) is the THz transmission spectrum collected by the lock-in amplifier in the 0.500 to 0.750 THz frequency range of the thin film deposited on the substrate, background (air or free space) and metal, respectively. THz transmission spectrum of the substrate were taken to normalize the thin film THz spectrum with respect to the background.

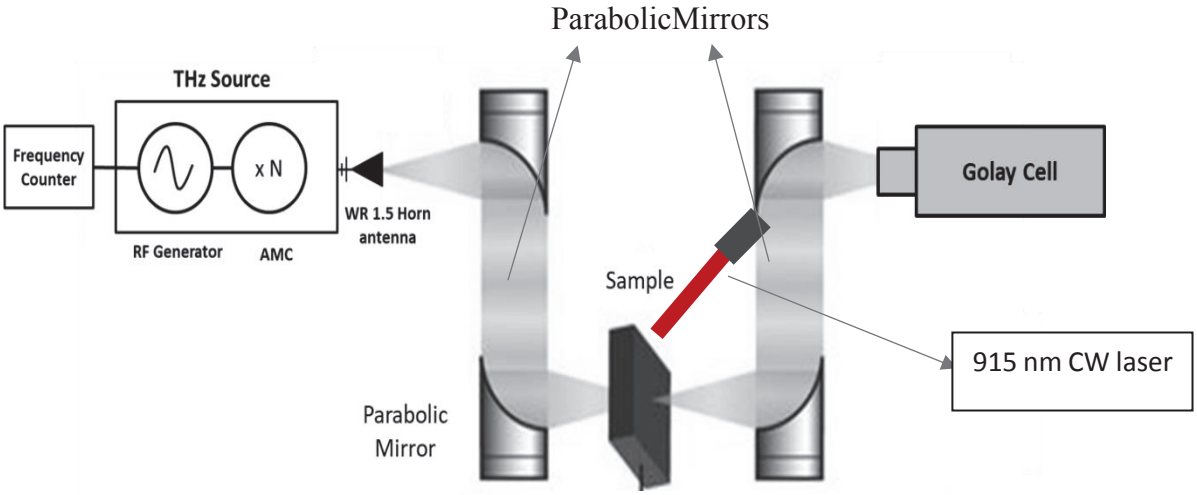

Figure 2.6. Schematic image of continuous wave THz system in THz Laboratory.

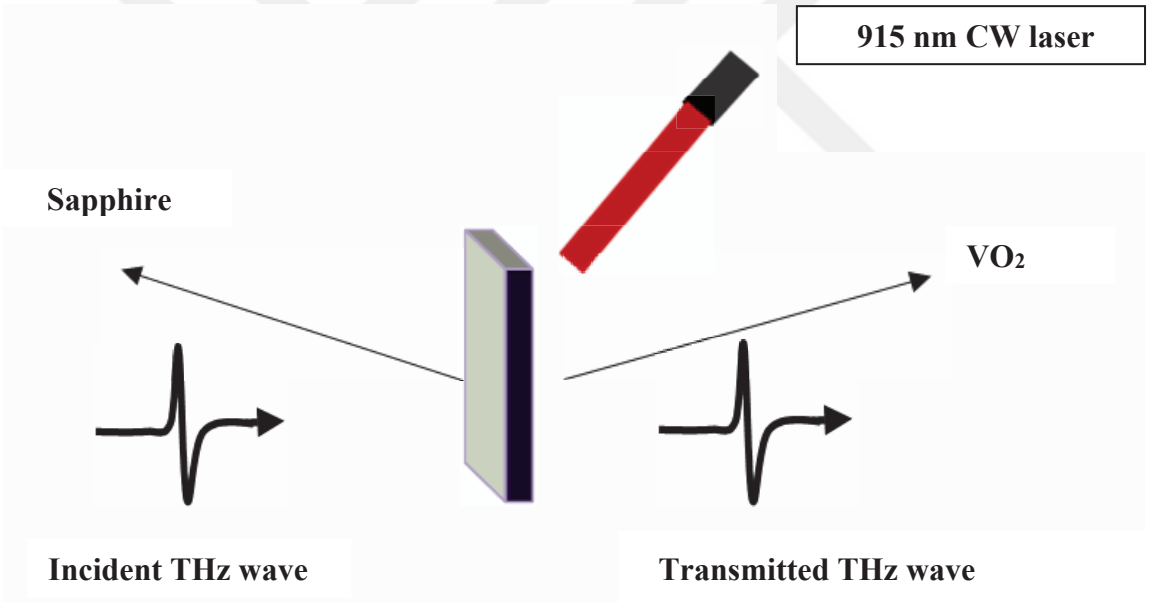

Figure 2.7. Illustration of sample triggering by CW laser while THz pass through.

After the full spectrum frequency data, the frequency where the amplitude of the transmitted wave is maximum is been used for THz wave switching as the IMT triggered by the laser. Within the 25 second since THz wave started to pass the sample through the parabolic mirrors, CW laser switched on. At that time transition started and sample started to block the THz radiation, within the 60 seconds CW laser is off then sample return back to insulator phase and allow THz radiation.

CHAPTER 3

RESULT AND DISCUSSION

3.1. Scanning Electron Microscopy (SEM) Analysis

Surface morphologies of two different VO_2 thin films which were deposited on c-cut sapphire at 1.60 % oxygen concentration with 280 nm thickness and 1.36 % oxygen concentration with 210 nm film thickness were investigated by using SEM (Fig.3.1). It can be seen that in Fig. 3.2, both thin films exhibit a similar crystal morphology that are composed of granular particles with aggregations and exhibit clear porous structure and thin films have no clear grain boundaries. Samples were grown at 550 °C and no post annealing were applied after the deposition.

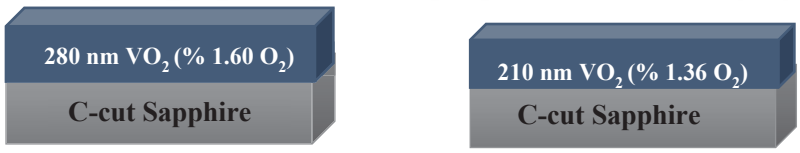

Figure 3.1. Schematic representation of VO_2 thin films on c-cut sapphire substrate with different thickness and oxygen concentration.

In Fig 3.3., it can be seen that the related cross-section images show obvious edges and thickness of the thin films were obtained from the cross-sections of samples.

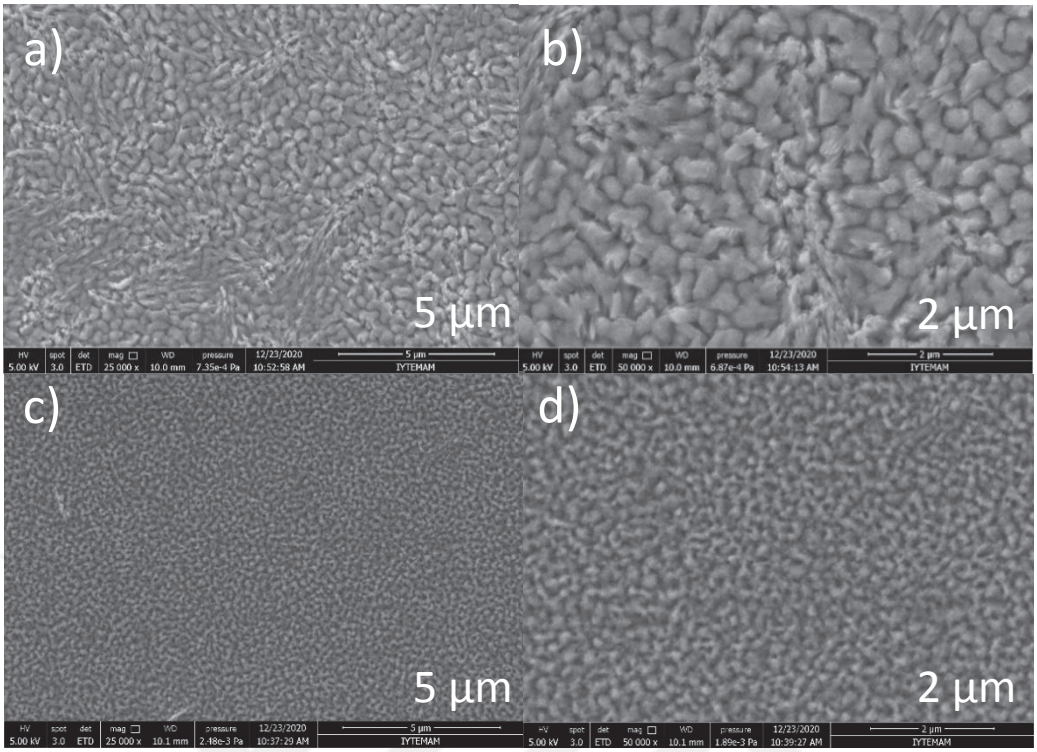

Figure 3.2. SEM images a)2 µm b) 5 µm of 210 nm VO_2 with 1.36 % oxygen concentration c)2 µm and d) 5 µm 280 nm VO_2 with 1.60 % oxygen concentration.

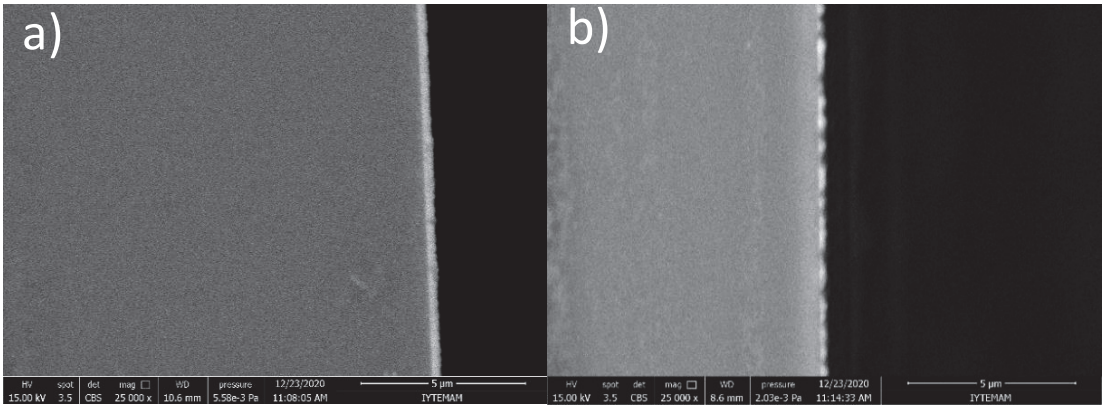

Figure 3.3. Cross-sectional image of VO_2 film a) 280 nm with 1.60 % oxygen concentration b) 210 nm with 1.36 % oxygen concentration.

3.2. X-Ray Difrraction Analysis

Crystallographic information of the VO_2 was obtained by XRD analysis. Structural properties of the samples were characterized by an X-ray diffractometer (XRD) (Philips X'Pert Pro) with CuKD radiation (O=0.154 nm). The XRD diffraction spectrum was collected from 10 to 90°. The corresponding XRD patterns on VO_2 thin films are shown in figure 3.7 and Fig 3.8. It was observed that all samples have secondary phases.

Fig 3.4 280 nm thickness with 1.60 % oxygen concentration, sample indicates that the major peaks are found at 38.12, 64.45 and 44.31, which may be related to the monoclinic vanadium dioxide phase and planes (020) (Zhao et al. 2012), the quadrangular crystalline aspect of vanadium dioxide (013) (AC et al. 2009) and (210) (Kim et al. 2014), respectively. The growth direction of vanadium dioxide on the c-cut sapphire substrate cannot be specific. The Bragg angles related to the (020) and (002) planes are equal (Yange et al. 2010). It can be shown that sample has secondary phases V_3O_7 and V_2O_5. Even though these VO_2 thin film seems to be inhomogeneous, thanks to strong peak at 38.1, sample shows good electrical characteristics of high quality VO_2 phase. In Fig 3.5 shows the XRD pattern of 210 nm thickness VO_2 with 1.36% oxygen rate. Peak at 42.2 and 64.8 related to (210) and (031) of monoclinic vanadium dioxide phase respectively. (Yang et al 2019). Peak at 44.6 corresponds to (012) plane of monoclinic VO2 phase (Zhang et al.2015). The peak around 40.15 with 2.24 angstrom d-spacing correspond to VO (111) plane (Kozen et al. 2017). Addition to vanadium oxide (VO) The sample has secondary phases $V_{14}O_{6,}$ V_2O_5 and V_3O_7 as well.

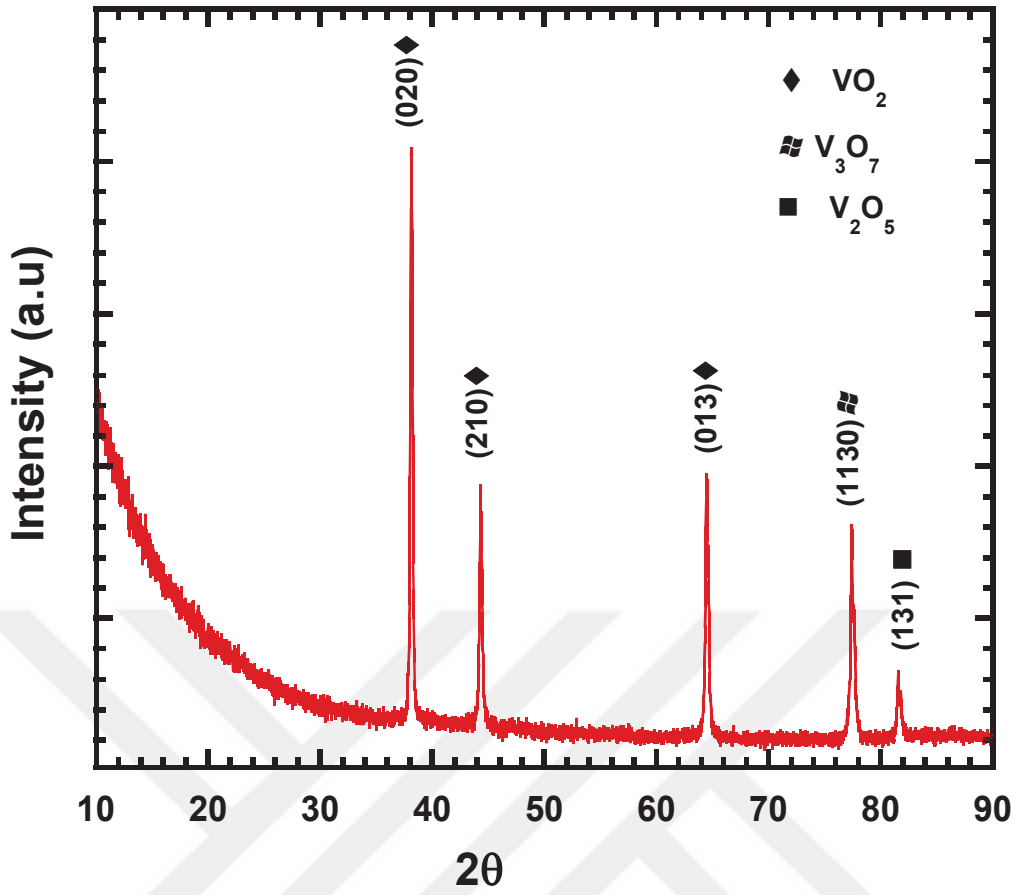

Figure 3.4. X-ray diffraction pattern of 280 nm VO_2 thin film with 1.60 % oxygen concentration.

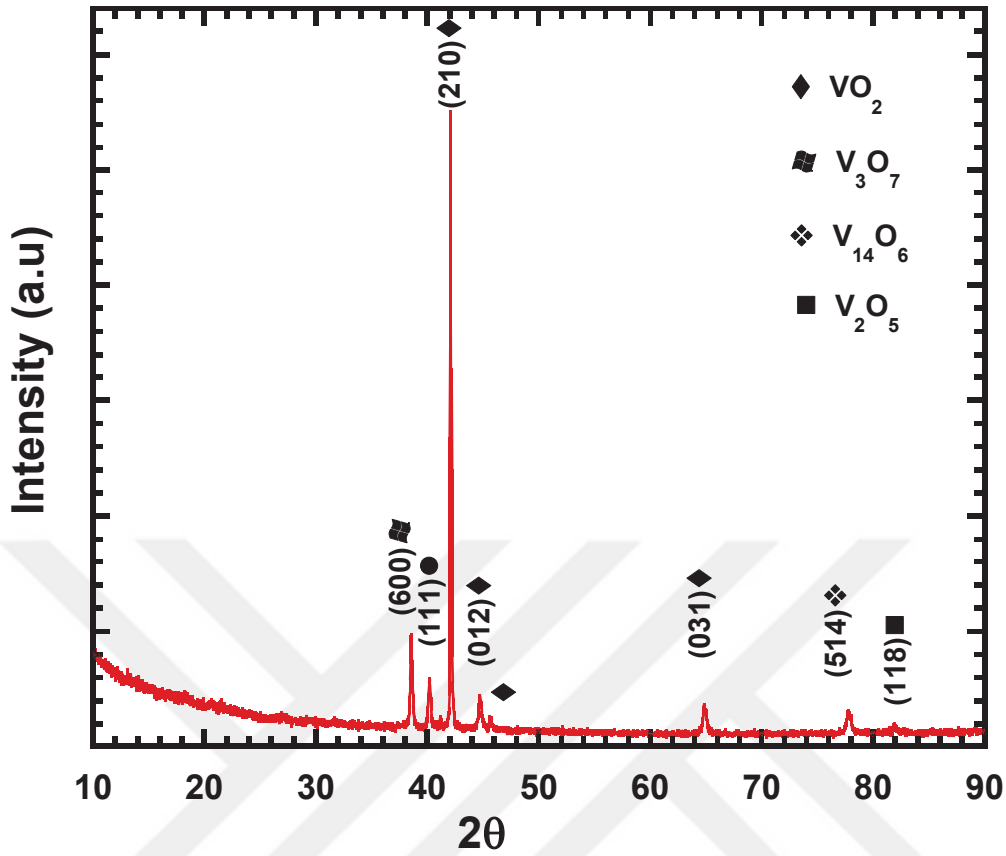

Fig 3.5. X-ray diffraction pattern of 210 nm VO_2 thin film with 1.36% oxygen concentration.

3.1 Raman Analysis

In order to obtain more information about the phase and crystallinity, Raman spectroscopy measurements were carried out for the two different VO_2 samples after the XRD and SEM results. Raman spectra of grown VO_2 thin films were obtained at room temperature shown in Fig 3.6. For VO_2, in the low temperature, monoclinic phase (M1), there are 18 modes. These are 9 A_g and 9 B_g active Raman modes (Schilbe 2002). The Raman modes which are 192, 224, 260, 311, 338, 389, 441 and 494 cm^{-1} belong to VO_2 vibration modes at 300 K (Vikhnin et al.1995). The peak which is at 617 cm^{-1} is the main peak of VO_2 phase and it belongs to V-V vibration mode (Piccirello et al. 2009). The

deposited VO_2 thin film with 280 nm thickness has strong peak at 617 cm^{-1} compared to the 210 nm VO_2 sample.

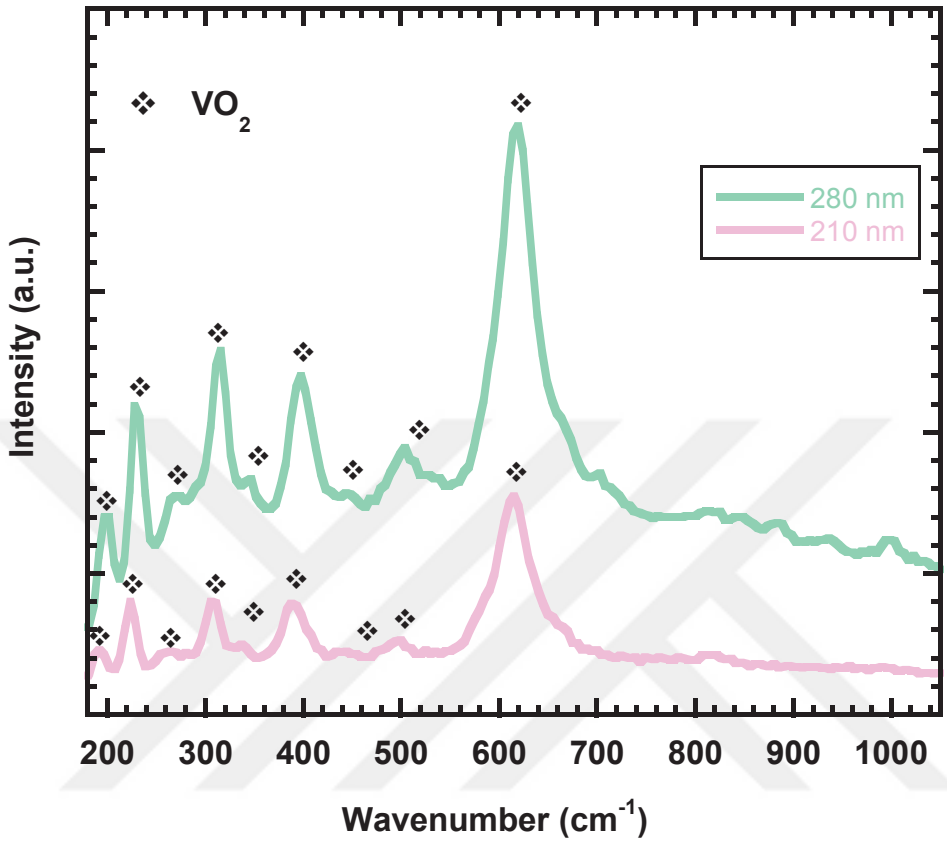

Figure 3.6. Raman spectra of grown VO_2 thin films with the thickness of 210 nm with 1.60 % O_2 and 310 nm with 1.36 % O_2 concentration.

3.1 Electrical Characterization

Electrical properties of deposited thin films were investigated. The resistivity of the samples between 20 °C – 100 °C was measured under vacuum in microprobe station. DC magnetron sputtered VO_2 samples show insulator-metal transition (IMT) around 68 °C. Various oxygen concentration and deposition time has been applied. The results indicate that oxygen concentration, deposition time and sputtering power effect the IMT characteristics of vanadium dioxide thin films.

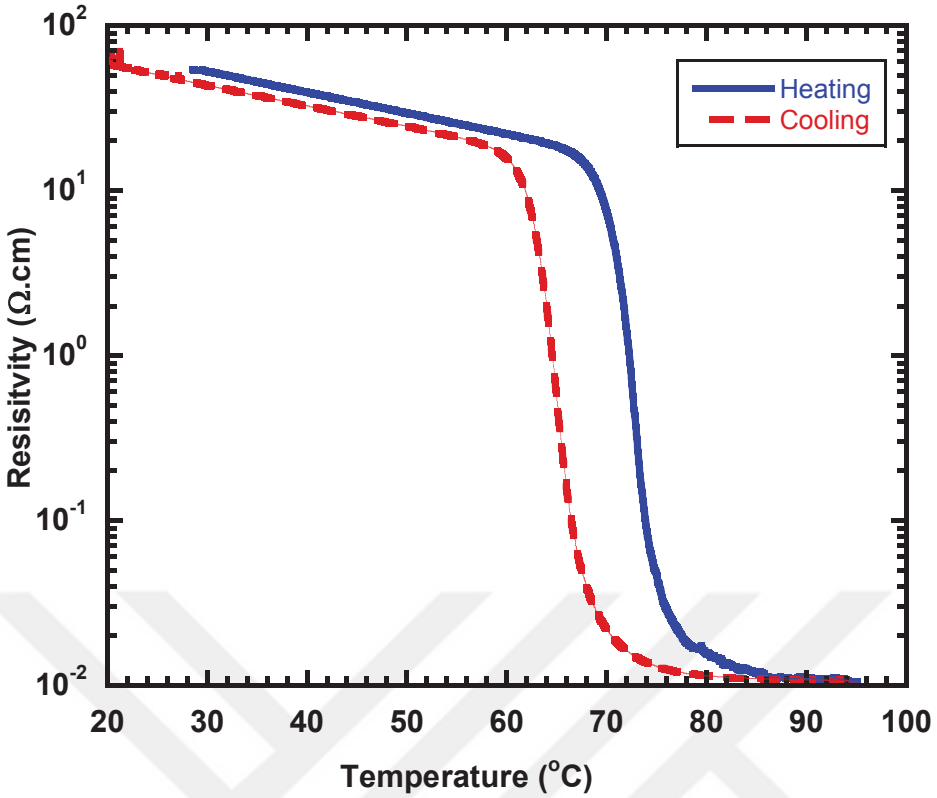

Figure 3.7. The resistivity depends on the temperature for vanadium dioxide sample with 1.60 % oxygen concentration.

The sample above in figure 3.6 shows the IMT characteristics with closely 4 orders of mag. of resistivity (3.8 decimal) change with hysteresis width around 6.5 ˚C and corresponding deposition parameters are listed in table 3.1.

Table 3.1. Deposition parameters of deposited vanadium dioxide where electrical behavior shown in figure 3.1.

Deposition parameters	
Sputtering DC power	70 watt
Argon/Oxygen ratio	136/2.20 sccm
Deposition time	60 minutes
Substrate temperature	550 ˚C

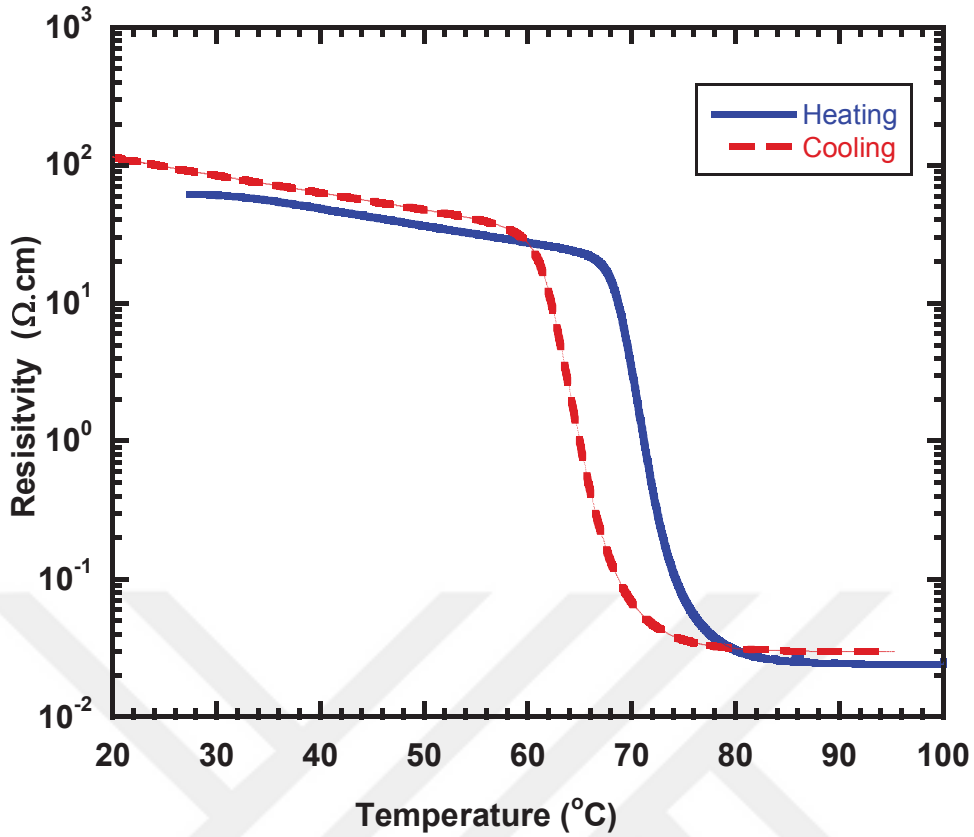

Figure 3.8. The resistivity depends on the temperature for vanadium dioxide sample with 1.36 % oxygen concentration

The sample above in figure 3.7 shows the IMT characteristics with closely 3 orders of magnitude of resistivity (2.9 decimal) change with hysteresis width around 7 °C and corresponding deposition parameters are listed in table 3.2.

Table 3.2. Deposition parameters of deposited vanadium dioxide where electrical behavior shown in figure 3.8 above.

Deposition parameters	
Sputtering DC power	50 Watt
Argon/Oxygen ratio	136/1.86 sccm
Deposition time	50 minutes
Substrate temperature	550 °C

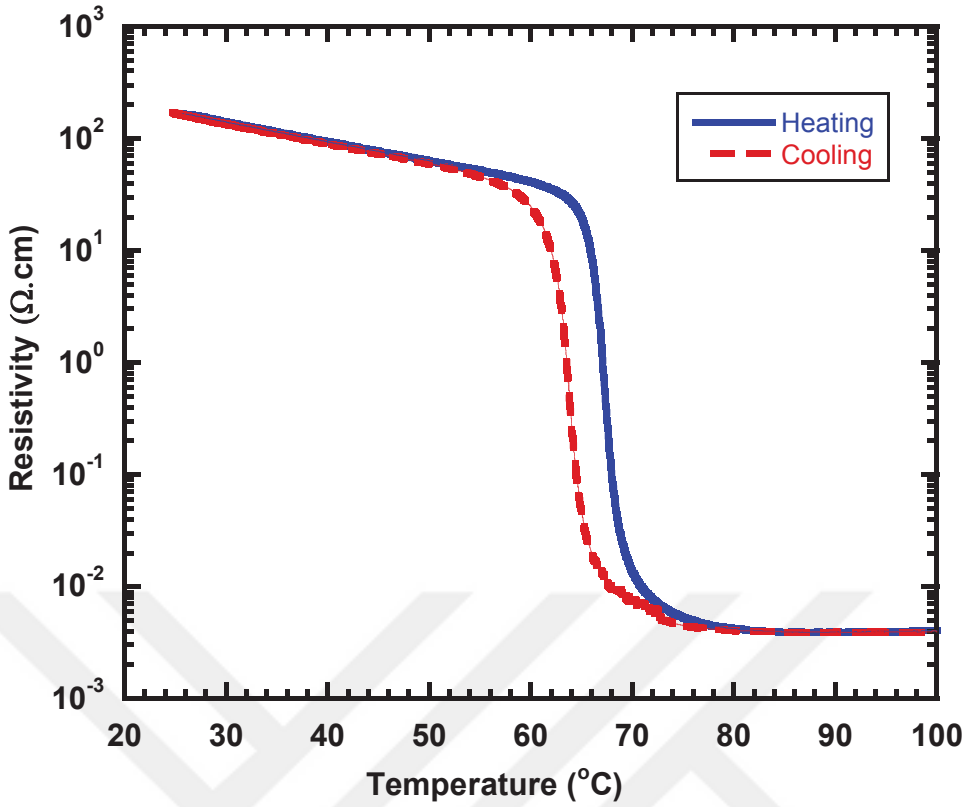

Figure 3.9. The resistivity depends on the temperature for VO_2 sample with 1.89 % O_2 concentration.

Table 3.3. Deposition parameters of deposited vanadium dioxide where electrical behavior shown in figure 3.9 above.

Deposition parameters	
Sputtering DC power	50 watt
Argon/oxygen ratio	136/2.58 sccm
Deposition time	50 minutes
Substrate temperature	550 °C

The sample above in figure 3.9 shows the IMT characteristics with closely 4 orders of magnitude of resistivity change with hysteresis width around 8.5 °C and corresponding deposition parameters are listed in Table 3.3. Broad hysteresis loop may indicate a randomized polycrystalline structure of the sample.

The sensitivity of the oxygen concentrations of thin films were investigated. It was shown in Fig 3.10 that a slight difference (0.01 %) in oxygen concentration of the thin films during the deposition causes a significant change in IMT behaviours of thin films. Vanadium dioxide with 2.49 % oxygen ratio has 4 order of magnitude of resistivity change during the transition. However, the magnitude of resistivity change decrease down to 2.5 order with decreasing oxygen ratio. This result indicates that oxygen concentration during the deposition plays an important role to obtain high quality vanadium dioxide phase. In figure 3.10 below shows the electrical behaviour of 3 deposited vanadium dioxide thin films which all grown for 70 minutes with 70 watt DC sputtering while heating from 20 to 100 °C.

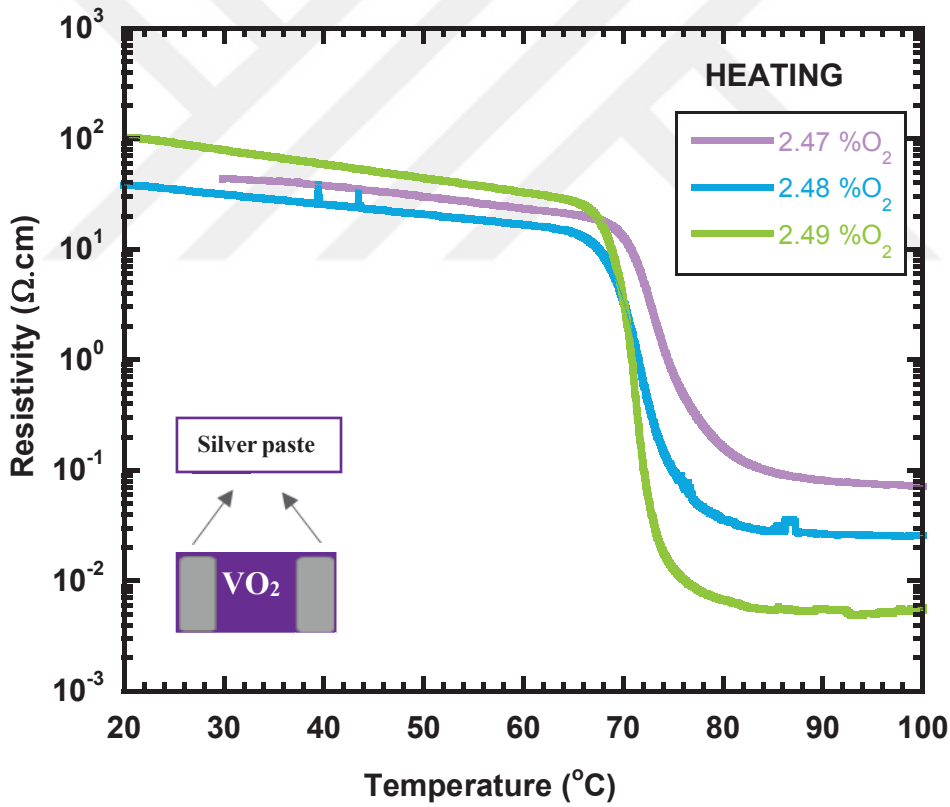

Figure 3.10. Electrical behaviour of 3 vanadium dioxide thin films with different oxygen concentration.

Aging behavior of the VO_2 thin films were also examined to the stability. Electrical measurements were performed of the same thin films just after the deposition process and one year later. In Fig. 3.11 and Fig. 3.12, the comparison of electrical properties between just deposited and one-year air exposed films are shown. During one-year, vacuum desicators have not been used and the thin films exposed air environment directly for one year and their resistivity change during the heating process compared. From the graphs below it can be seen that in their heating graphic, a slight increase in resistivity in thin films exists after one year air exposition. Despite the change in resistivity the order of magnitude of resistivity change in IMT remains the same. This indicates that a slight change in resistivity caused by contact resistance.

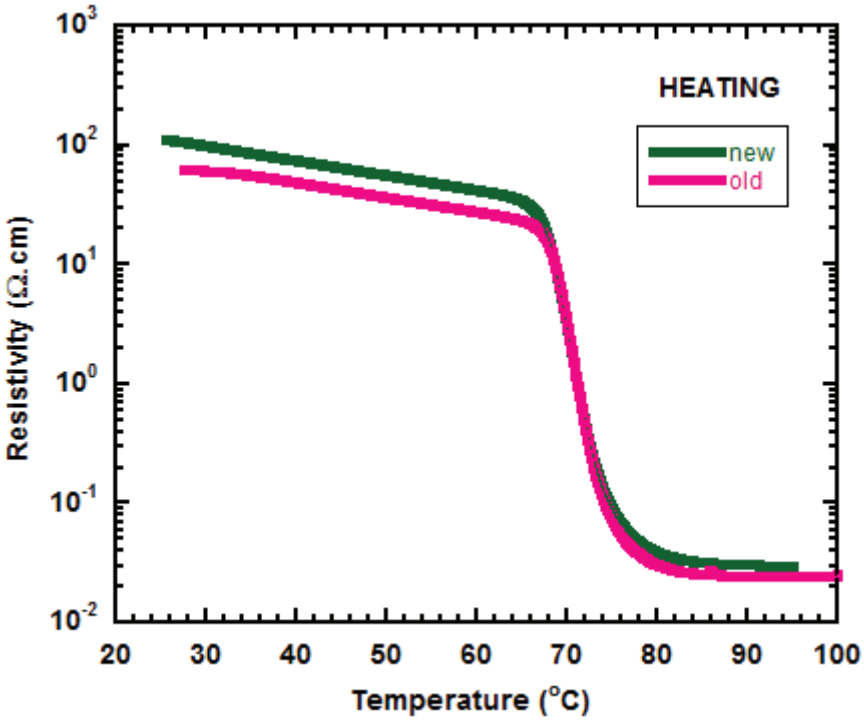

Figure 3.11. Comparison of electrical properties between freshly deposited and one year air exposed vanadium dioxide film grown with 2.60 % oxygen concentration films.

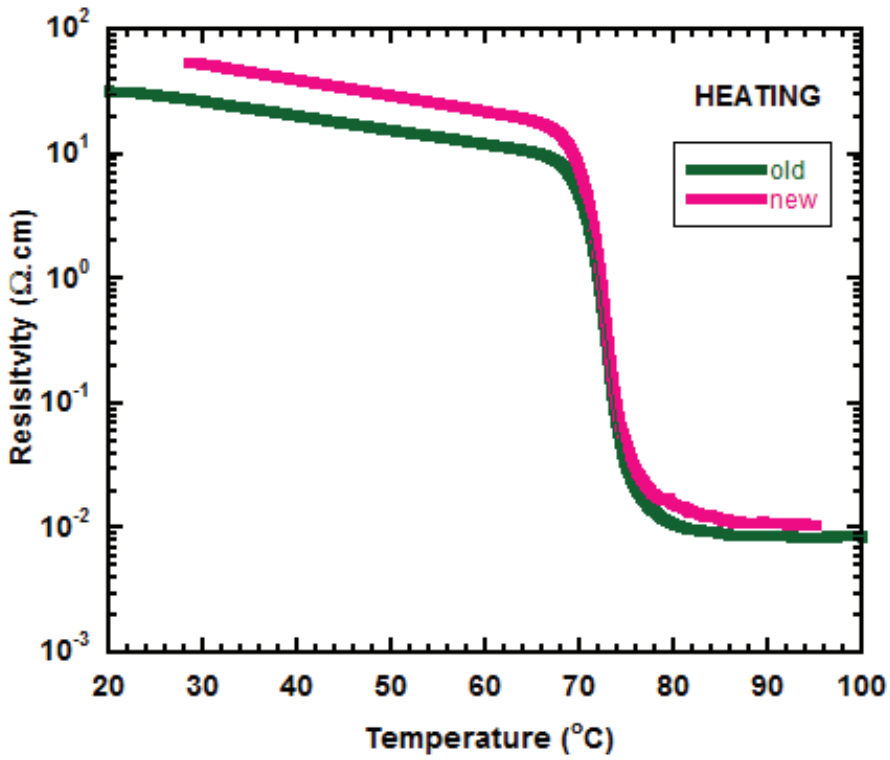

Figure 3.12. Comparison of electrical properties between freshly deposited and one year air exposed thin film grown with 2.40 % oxygen concentration.

3.2. Terahertz Characterization

In this part, terahertz modulation characteristics of vanadium dioxide thin films which have different magnitude of change in resistivity during the IMT has been investigated. The maximum transition terahertz frequency of thin films was determined from the full spectrum graph as shown below. Fig 3.14 shows the corresponding transition amplitude of terahertz wave passing through the vanadium dioxide samples grown on c-cut sapphire between 500 – 750 GHz at 20 °C. From the full spectrum graph in Fig 3.14, frequency where the terahertz transmission is maximum was obtained at room temperature.

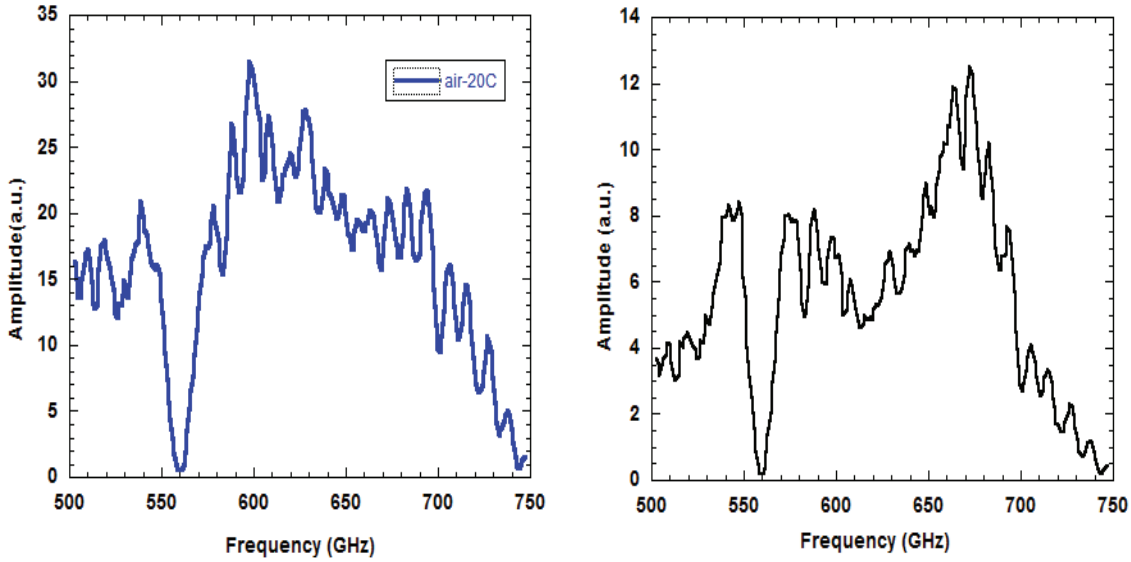

Figure 3.13. Full spectrum graph of a) **air** b) **c-cut sapphire (Al_2O_3) +air** substrate at 20 ˚C

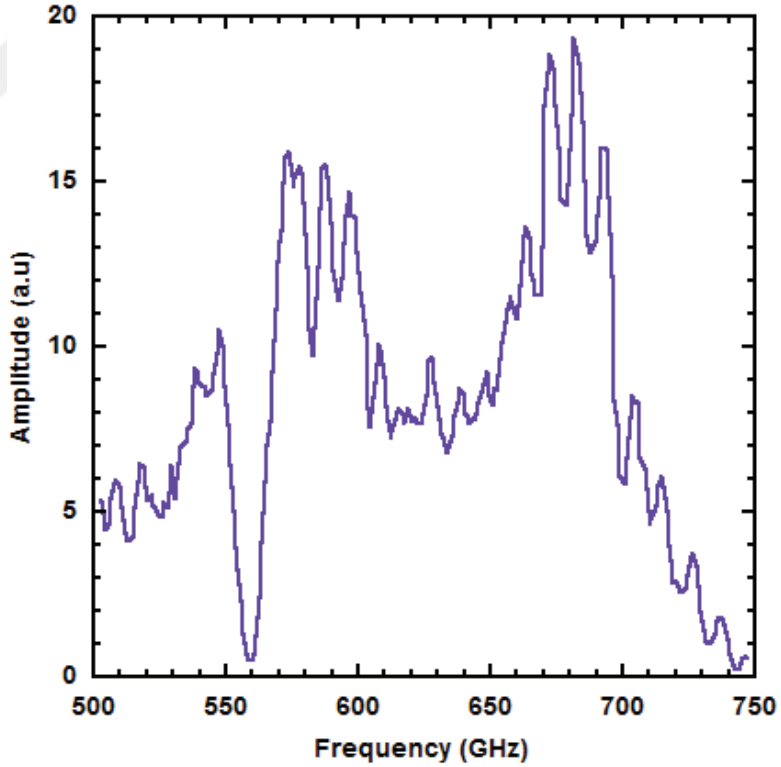

Figure 3.14. Full spectrum graph of 280 nm **VO_2** + **Al_2O_3** grown with 70W sputtering power, 1.60 % oxygen concentration

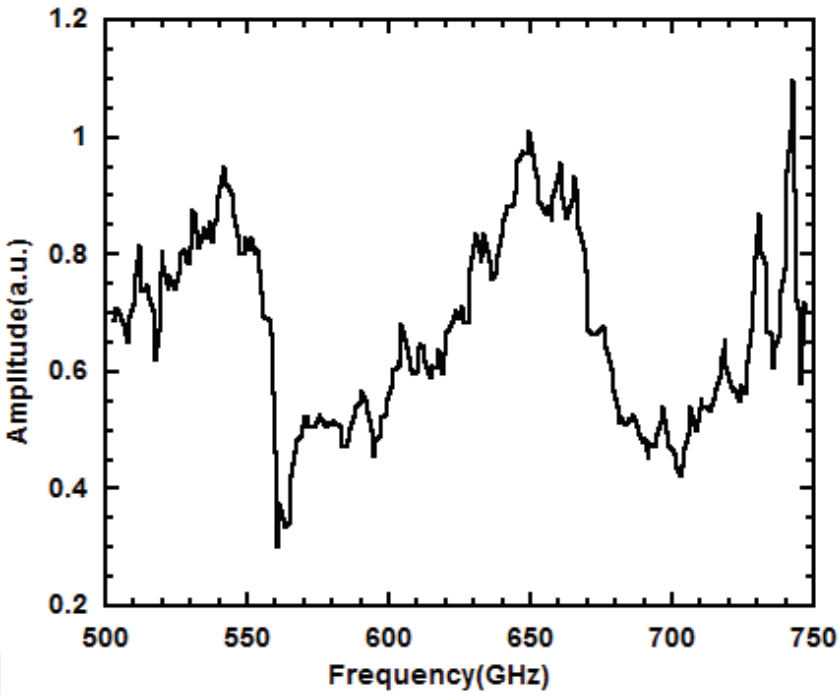

Figure 3.15. Full spectrum graph of 280 nm **VO_2** grown with 70W sputtering power with 1.60 % oxygen concentration.

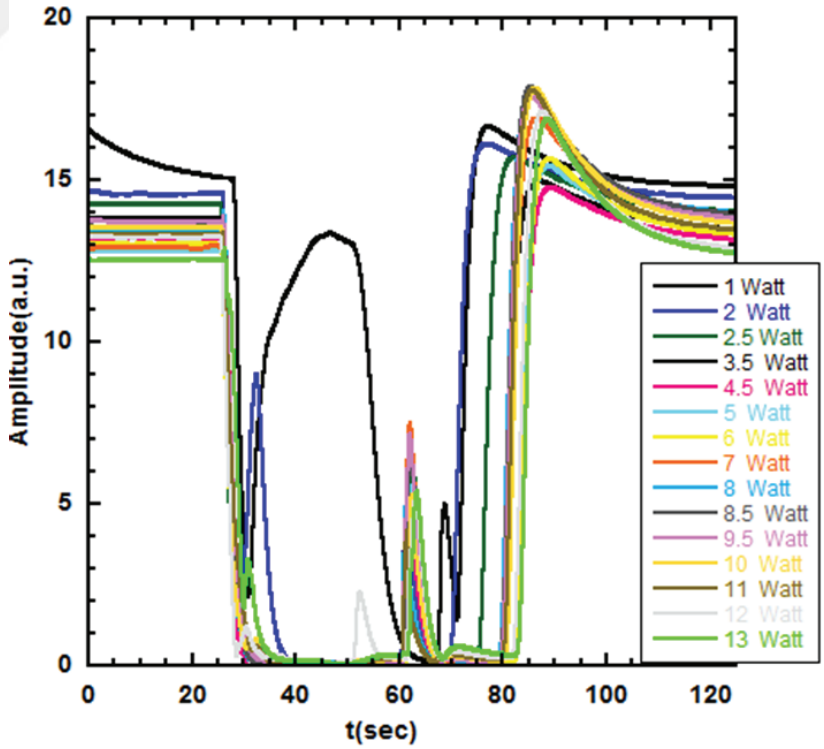

Figure 3.16. THz modulation characteristic of 280 nm VO_2 grown with 70W sputtering power with 1.60 % oxygen concentration.

Fig 3.16 shows the THz modulation behaviour of vanadium dioxide sample at 584 GHz which obtained from the full spectrum graph shown in fig 3.14. Sample has ΔR = $10^{3.7}$ change during the transition from semiconducting phase to metallic phase. Within 25 second, continuous wave (CW) 915 nm laser switched on in order to trigger the IMT behavior of the VO_2 sample. Within the 60 seconds laser switched off and sample started to cool down. Various laser powers were applied as shown in Fig 3.16. It can be seen from the graph that with 1 watt laser power, no expected transition behaviour was observed. With 2 watt laser power, sample started to block the terahertz wave while triggered by the laser. Below the critical temperature VO_2 film is transparent for THz radiation and above the critical temperature VO_2 film reflects THz radiation. In other words, above the critical temperature VO_2 thin film is in the metallic state and below the critical temperature it is in insulating state. This experimental procedure followed for the samples which has different ΔR values as well.

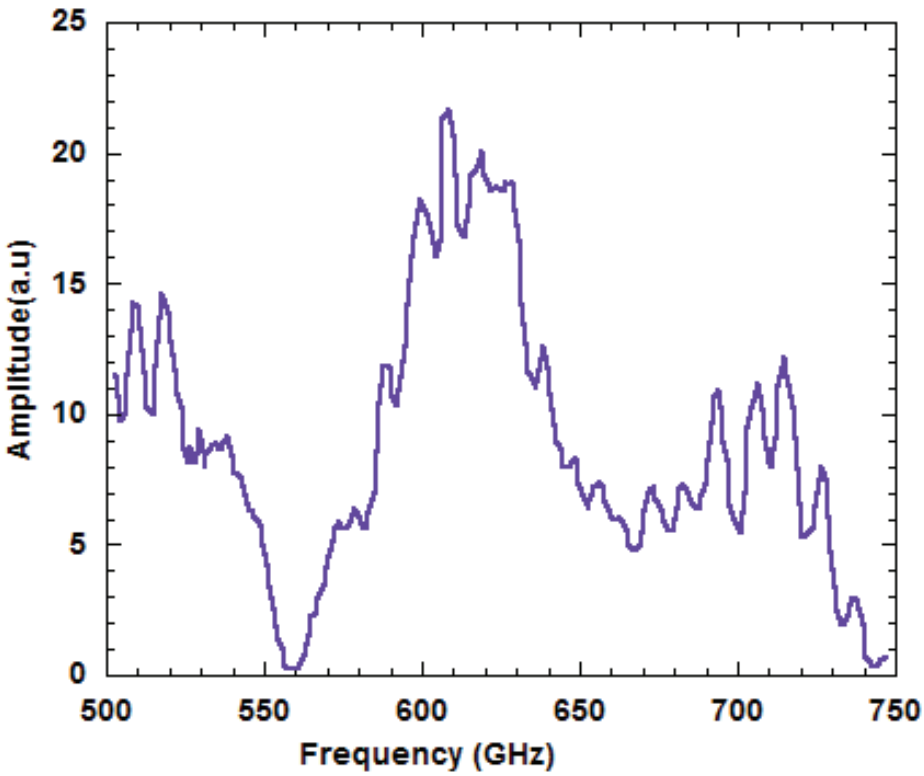

Figure 3.17. Full spectrum graph of **VO_2+Al_2O_3** grown with 70W sputtering power with 1.89 % oxygen concentration.

In figure 3.17 above shows the full spectrum graph of VO_2+Al_2O_2 another sample with 1.89 % which has different $\Delta R = 10^3$. The figure 3.18 below belongs to VO_2 sample with 1.89 % oxygen concentration without sapphire substrate effect. From the full spectrum graph of VO_2+Al_2O_2 in figure 3.17 maximum transmission amplituted was obtained.

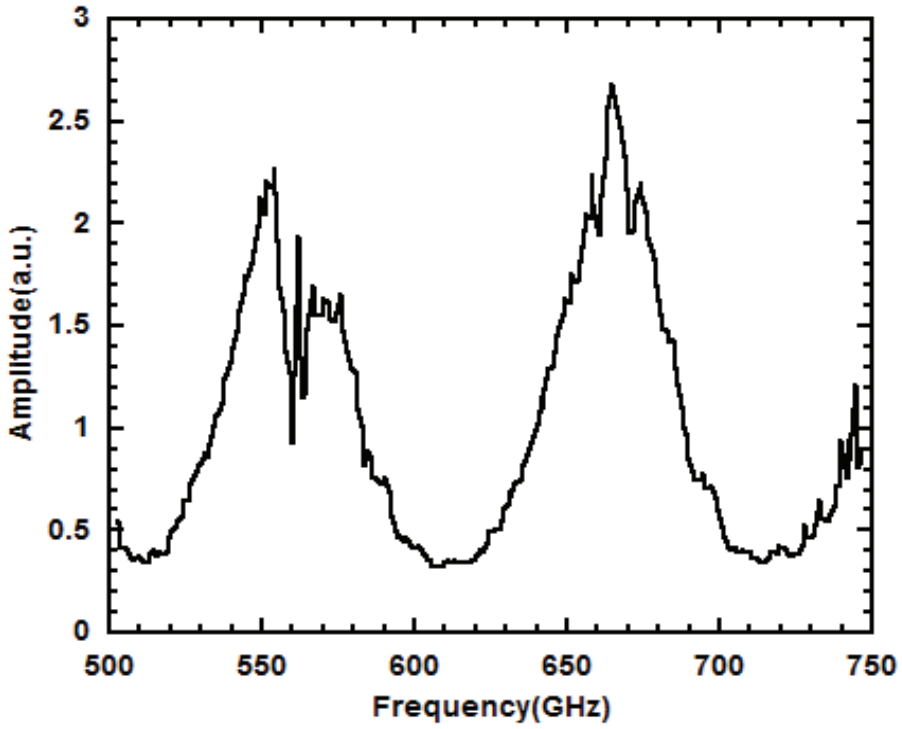

Figure 3.18. Full spectrum graph of **VO_2** grown with 70W sputtering power 1.89 % oxygen concentration, 60 minutes deposition time.

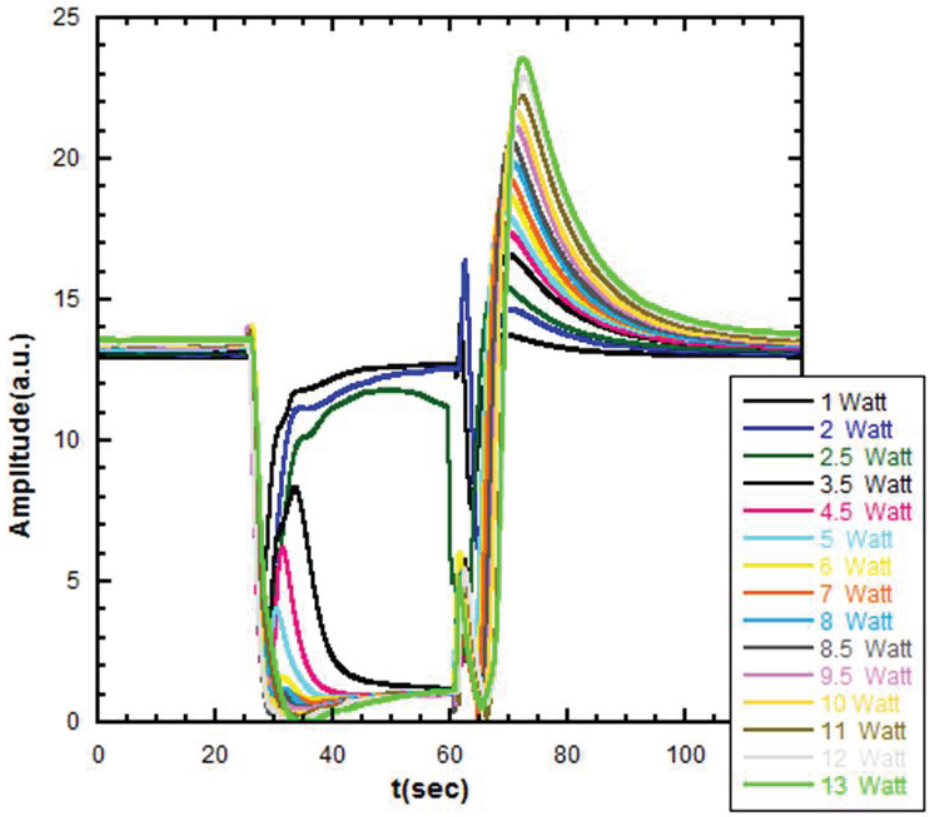

Figure 3.19. THz modulation characteristic of VO_2 grown with 70W sputtering power, 1.89 % oxygen concentration.

In Fig 3.19 above shows the transmission behaviour of the VO_2 thin films which has $\Delta R = 10^3$ value during the transition. The measurement was performed at 612 GHz where terahertz transmission was maximum shown in Fig. 3.17. In contrast to the Fig 3.16, obvious transmission behaviour was started to observe with the 3.5 W laser power. This difference can be caused by the different ΔR values of the samples.

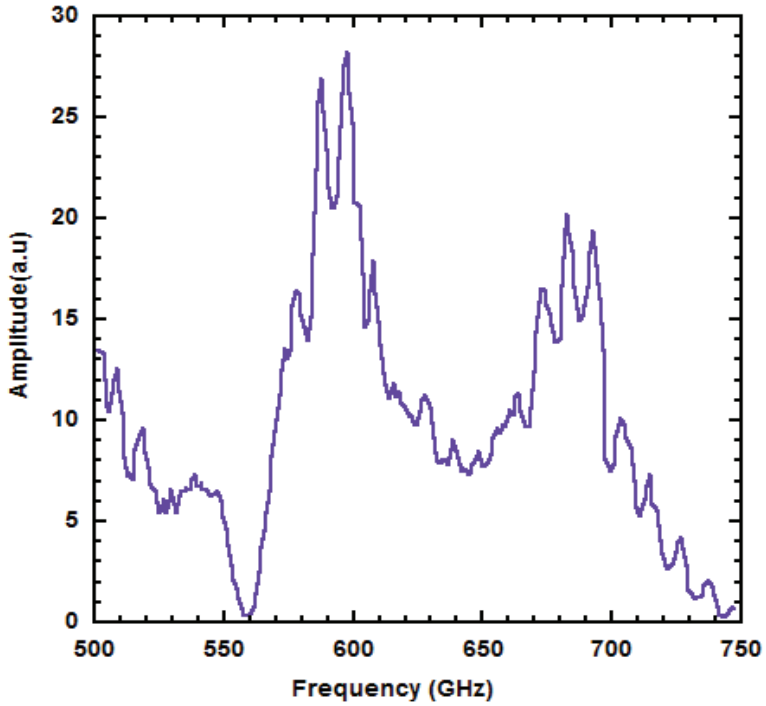

Figure 3.20. Full spectrum graph of **VO_2+Al_2O_3** grown with 50W sputtering power 1.36 % oxygen concentration, 50 minutes deposition time.

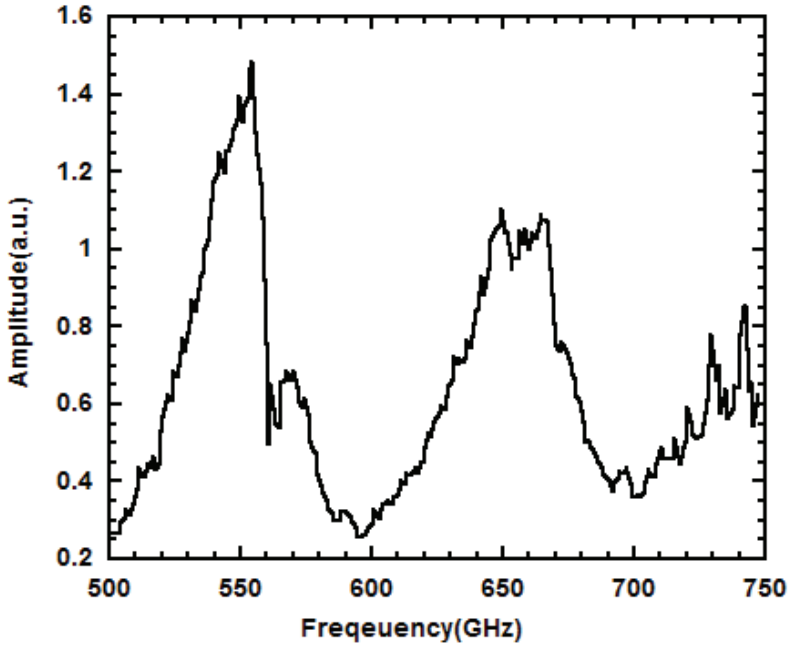

Figure 3.21. Full spectrum graph of **VO_2** grown with 50W sputtering power 1.36 oxygen concentration, 50 minutes deposition time.

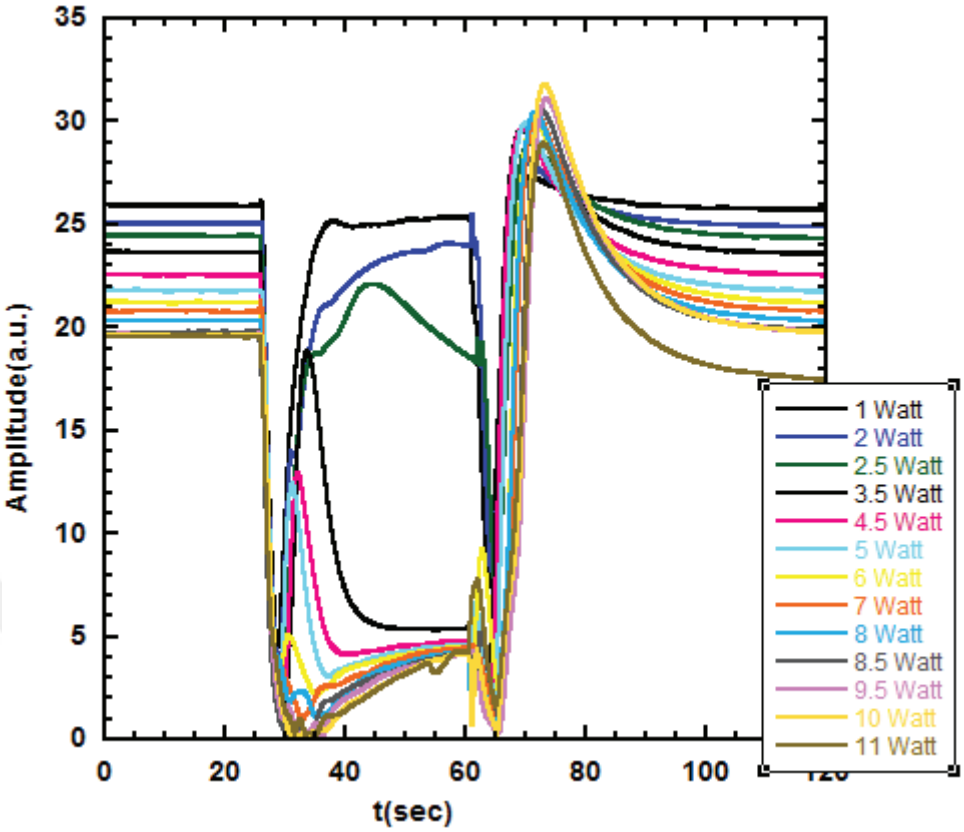

Figure 3.22. THz modulation characteristic of VO_2 with 50W sputtering power with 1.36 % oxygen concentration.

Fig 3.22 shows the THz wave transmission behaviour of VO_2 sample with $\Delta R = 10^{2.5}$ during the transition. In room temperature, in order to obtain maximum transmission amplitude, between 500 – 750 GHz full spectrum measurement was performed. From the Fig 3.20 maximum frequency obtained at 593 GHz. Then at 593 GHz, transmission behaviour characteristics was observed while IMT triggered by the laser. It can be seen that laser power below than 3.5 watt no obvious transmission behaviors was observed. In 3.5 W laser power, VO_2 sample started to reflect the terahertz waves.

CHAPTER 4

CONCLUSION

İnsulator- metal transition observed in vanadium dioxide (VO_2) samples at 68 $^{\circ}$C. At the temperature of insulator-metal transition (IMT), change in the crystal structure flowed by electrical and optical change in VO_2 with a change in crystal structure. Among VO_x compounds, VO_2 has the lowest transition temperature which is close to the room temperature. This property makes VO_2 quite practical for being used switched electronics.

In this work, DC magnetron sputtering method for VO_2 thin film synthesis was used thanks to good adhesion, homogeneity and controllability.

For the thin film fabrication, optimization of the system conditions were performed. In order to minimize the concentration of the secondary phases, optimum deposition parameters were investigated. The effect of sputtering power and oxygen stoichiometry were examined. C-cut sapphire was chosen for a substrate because of its good thermal conductivity. Deposition with various oxygen concentrations and sputtering powers were performed. In micro probe station, electrical properties of deposited thin films were investigated. Thin films which has higher resistivity change during the transition were chosen for terahertz characterization. In continuous wave (CW) terahertz system, the modulation characteristics of the thin films performed. It has been observed that in semiconducting phase VO_2 lets THz wave propagation whereas in metallic phase it blocks the THz radiation. This ability to switch THz waves thanks to IMT phenomena of VO_2 make it a promising material in application of high date rate wireless communication.

REFERENCES

Alaboz, H.; Demirhan, Y.; Yuce, H.; Aygun, G.; Ozyuzer, L. Comparative Study of Annealing and Gold Dopant Effect on DC Sputtered Vanadium Oxide Films for Bolometer Applications. *Optical and Quantum Electronics* **2017**, *49*.

Barani, Z.; Kargar, F.; Godziszewski, K.; Rehman, A.; Yashchyshyn, Y.; Rumyantsev, S.; Cywiński, G.; Knap, W.; Balandin, A. A. Graphene Epoxy-Based Composites as Efficient Electromagnetic Absorbers in the Extremely High-Frequency Band. *ACS Applied Materials & Interfaces* **2020**, *12*, 28635–28644.

Cao, J.; Ertekin, E.; Srinivasan, V.; Fan, W.; Huang, S.; Zheng, H.; Yim, J. W.; Khanal, D. R.; Ogletree, D. F.; Grossman, J. C.; *et al.* Strain Engineering and One-Dimensional Organization of Metal–Insulator Domains in Single-Crystal Vanadium Dioxide Beams. *Nature Nanotechnology* **2009**, *4*, 732–737.

Cavalleri, A.; Dekorsy, T.; Chong, H. H.; Kieffer, J. C.; Schoenlein, R. W. Evidence for a Structurally-Driven Insulator-to-Metal Transition inVO2: A View from the Ultrafast Timescale. *Physical Review B* **2004**, *70*.

Cavalleri, A.; Rini, M.; Chong, H. H.; Fourmaux, S.; Glover, T. E.; Heimann, P. A.; Kieffer, J. C.; Schoenlein, R. W. Band-Selective Measurements of Electron Dynamics inVO2Using Femtosecond Near-Edge X-Ray Absorption. *Physical Review Letters* **2005**, *95*.

Chang, T.-C.; Cao, X.; Bao, S.-H.; Ji, S.-D.; Luo, H.-J.; Jin, P. Review on Thermochromic Vanadium Dioxide Based Smart Coatings: from Lab to Commercial Application. *Advances in Manufacturing* **2018**, *6*, 1–19.

Crunteanu, A.; Leroy, J.; Humbert, G.; Ferachou, D.; Orlianges, J.-C.; Champeaux, C.; Blondy, P. Tunable Terahertz Metamaterials Based on Metal-Insulator Phase Transition of VO2 Layers. *2012 IEEE/MTT-S International Microwave Symposium Digest* **2012**

Das, R. S.; Agrawal, Y. K. Raman Spectroscopy: Recent Advancements, Techniques and Applications. *Vibrational Spectroscopy* **2011**, *57*, 163–176

Donev, E.U. Metal-semiconductor Transitions in Nanoscale Vanadium Dioxide Thin Films, Subwavelength Holes, and Nanoparticles. **2008**, Vanderbilt University.

Ferguson, B.; Zhang, X.-C. Materials for Terahertz Science and Technology. *Nature Materials* **2002**, *1*, 26–33.

Fillingham, P. J. Domain Structure and Twinning in Crystals of Vanadium Dioxide. *Journal of Applied Physics* **1967**, *38*, 4823–4829.

Gervais, F.; Kress, W. Lattice Dynamics of Oxides with Rutile Structure and Instabilities at the Metal-semiconductor Phase Transitions ofNbO2andVO2. *Physical Review B* **1985**, *31*, 4809–4814.

Goodenough, J. B. Anomalous Properties of the Vanadium Oxides. *Annual Review of Materials Science* **1971**, *1*, 101–138

Gopalan, P.; Sensale-Rodriguez, B. 2D Materials for Terahertz Modulation. *Advanced Optical Materials* **2019**, *8*, 1900550.

Griffiths, C. H.; Eastwood, H. K. Influence of Stoichiometry on the Metal-semicondcutor Transition in Vanadium Dioxide. *Journal of Applied Physics* **1974**, *45*, 2201–2206.

Imada, M.; Fujimori, A.; Tokura, Y. Metal-Insulator Transitions. *Reviews of Modern Physics* **1998**, *70*, 1039–1263

Kakiuchida, H.; Jin, P.; Nakao, S.; Tazawa, M. Optical Properties of Vanadium Dioxide Film during Semiconductive–Metallic Phase Transition. *Japanese Journal of Applied Physics* **2007**, *46*.

Kim, H.-T.; Chae, B.-G.; Youn, D.-H.; Maeng, S.-L.; Kim, G.; Kang, K.-Y.; Lim, Y.-S. Mechanism and Observation of Mott Transition in VO2-Based Two- and Three-Terminal Devices. *New Journal of Physics* **2004**, *6*, 52–52

Kim, H.; Charipar, N.; Osofsky, M.; Qadri, S. B.; Piqué, A. Optimization of the Semiconductor-Metal Transition in VO2 Epitaxial Thin Films as a Function of Oxygen Growth Pressure. *Applied Physics Letters* **2014**, *104*, 081913

Kozen, A. C.; Joress, H.; Currie, M.; Anderson, V. R.; Eddy, C. R.; Wheeler, V. D. Structural Characterization of Atomic Layer Deposited Vanadium Dioxide. *The Journal of Physical Chemistry C* **2017**, *121*, 19341–19347.

Landy, N. I.; Bingham, C. M.; Tyler, T.; Jokerst, N.; Smith, D. R.; Padilla, W. J. Design, Theory, and Measurement of a Polarization-Insensitive Absorber for Terahertz Imaging. *Physical Review B* **2009**, *79*

Lazarovits, B.; Kim, K.; Haule, K.; Kotliar, G. Effects of Strain on the Electronic Structure ofVO2. *Physical Review B* **2010**, *81*.

Leroy, J.; Crunteanu, A.; Bessaudou, A.; Cosset, F.; Champeaux, C.; Orlianges, J.-C. High-Speed Metal-Insulator Transition in Vanadium Dioxide Films Induced by an Electrical Pulsed Voltage over Nano-Gap Electrodes. *Applied Physics Letters* **2012**, *100*, 213507

Lopez, R.; Boatner, L. A.; Haynes, T. E.; Feldman, L. C.; Haglund, R. F. Synthesis and Characterization of Size-Controlled Vanadium Dioxide Nanocrystals in a Fused Silica Matrix. *Journal of Applied Physics* **2002**, *92*, 4031–4036.

Morin, F. J. Oxides Which Show a Metal-to-Insulator Transition at the Neel Temperature. *Physical Review Letters* **1959**, *3*, 34–36.

Mott, N. F. Metal-Insulator Transitions, Taylor and Francis. **1990**. New York

Namai, A.; Sakurai, S.; Nakajima, M.; Suemoto, T.; Matsumoto, K.; Goto, M.; Sasaki, S.; Ohkoshi, S.-ichi. Synthesis of an Electromagnetic Wave Absorber for High-Speed Wireless Communication. *Journal of the American Chemical Society* **2009**, *131*, 1170–1173.

Nouman, M. T.; Kim, H.-W.; Woo, J. M.; Hwang, J. H.; Kim, D.; Jang, J.-H. Terahertz Modulator based on Metamaterials integrated with Metal-İnsulator-Metal Varactors https://www.nature.com/articles/srep26452/ (accessed Feb 21, 2021

OAK RIDGE LABORATORY https://science.energy.gov/bes/highlights/2015/bes-2015-03-a/. (accessed Feb 21, 2021).

Ouchi, T.; Kajiki, K.; Koizumi, T.; Itsuji, T.; Koyama, Y.; Sekiguchi, R.; Kubota, O.; Kawase, K. Terahertz Imaging System for Medical Applications and Related High Efficiency Terahertz Devices. *Journal of Infrared, Millimeter, and Terahertz Waves* **2013**, *35*, 118–130.

Ozyuzer, L.; Koshelev, A. E.; Kurter, C.; Gopalsami, N.; Li, Q.; Tachiki, M.; Kadowaki, K.; Yamamoto, T.; Minami, H.; Yamaguchi, H.; *et al.* Emission of Coherent THz Radiation from Superconductors. *Science* **2007**, *318*, 1291–1293

Piccirillo, C.; Binions, R.; Parkin, I. P. Synthesis and Functional Properties of Vanadium Oxides: V2O3, VO2, and V2O5 Deposited on Glass by Aerosol-Assisted CVD. *Chemical Vapor Deposition* **2007**, *13*, 145–151

Rice, T. M.; Launois, H.; Pouget, J. P. Comment on "VO2: Peierls or Mott-Hubbard? A View from Band Theory". *Physical Review Letters* **1994**, *73*, 3042–3042.

Ruzmetov, D.; Zawilski, K. T.; Narayanamurti, V.; Ramanathan, S. Structure-Functional Property Relationships in Rf-Sputtered Vanadium Dioxide Thin Films. *Journal of Applied Physics* **2007**, *102*, 113715

Schilbe, P. Raman Scattering in VO2. *Physica B: Condensed Matter* **2002**, *316-317*, 600–602

Soltani, M.; Chaker, M.; Haddad, E.; Kruzelecky, R. V.; Margot, J. Effects of Ti–W Codoping on the Optical and Electrical Switching of Vanadium Dioxide Thin Films Grown by a Reactive Pulsed Laser Deposition. *Applied Physics Letters* **2004**, *85*, 1958–1960.

Soltani, M.; Kaye, A. B. Properties and Applications of Thermochromic Vanadium Dioxide Smart Coatings. *Intelligent Coatings for Corrosion Control* **2015**, 461–490.

Stanjek, H.; Häusler, W. Basics of x-Ray Diffraction. *Hyperfine Interactions* **2004**, *154*, 107–119.

SURA (Southeastern Universities Research Association) http://www.sura.org/commercialization/terahertz.html#EMS_Chart. (accessed Feb 21, 2021).

Tomczak, J. M.; Aryasetiawan, F.; Biermann, S. Effective Bandstructure in the Insulating Phase versus Strong Dynamical Correlations in metallic VO2. *Physical Review B* **2008**, *78*.

Turrell, G. The Raman Effect. *Raman Microscopy* **1996**, 1–25.

Vikhnin, V. S.; Goncharuk, I. N.; Davydov, V. Yu.; Chudnovskii, F.A.; Shadrin, E. B. Raman Spectra of the High-temperature Phase of Vanadium Dioxide and Model of Structural Transformations near the Metal-semiconductor Phase Transition. *Physics of the Solid State* **1995,** 37-12.

Wang, X. J.; Li, H. D.; Fei, Y. J.; Wang, X.; Xiong, Y. Y.; Nie, Y. X.; Feng, K. A. XRD and Raman Study of Vanadium Oxide Thin Films Deposited on Fused Silica Substrates by RF Magnetron Sputtering. *Applied Surface Science* **2001**, *177*, 8–14.

Weber, C.; O'Regan, D. D.; Hine, N. D.; Payne, M. C.; Kotliar, G.; Littlewood, P. B. Vanadium Dioxide: A Peierls-Mott Insulator Stable against Disorder. *Physical Review Letters* **2012**, *108*

Wentzcovitch, R. M.; Schulz, W. W.; Allen, P. B. VO2: Peierls or Mott-Hubbard? A View from Band Theory. *Physical Review Letters* **1994**, *72*, 3389–3392.

Wu, J.; Liou, L. Room Temperature Photo-Induced Phase Transitions of VO2 Nanodevices. *Journal of Materials Chemistry* **2011**, *21*, 5499

Yang, R.; Wu, Z.; Ji, C.; Wu, X.; Xiang, Z.; Zhang, F.; Li, W.; Wang, J.; Dong, X.; Jiang, Y. Far-IR Transmittance and Metal–Insulator Phase Transition Properties of VO2 Films Using Al2O3 as Buffer Layer. *Journal of Materials Science: Materials in Electronics* **2019**, *30*, 6448–6458.

Yi, X.; Chen, C.; Liu, L.; Wang, Y.; Xiong, B.; Wang, H.; Chen, S. A New Fabrication Method for Vanadium Dioxide Thin Films Deposited by Ion Beam Sputtering. *Infrared Physics & Technology* **2003**, *44*, 137–141

Yuce, H.; Alaboz, H.; Demirhan, Y.; Ozdemir, M.; Ozyuzer, L.; Aygun, G. Investigation of Electron Beam Lithography Effects on Metal–Insulator Transition Behavior of Vanadium Dioxide. *Physica Scripta* **2017**, *92*, 114007

Zhang, H.; Wu, Z.; Niu, R.; Wu, X.; he, Q.; Jiang, Y. Metal–Insulator Transition Properties of Sputtered Silicon-Doped and Un-Doped Vanadium Dioxide Films at Terahertz Range. *Applied Surface Science* **2015**, *331*, 92–97

Zhang, L.-L.; Wang, W.-M.; Wu, T.; Feng, S.-J.; Kang, K.; Zhang, C.-L.; Zhang, Y.; Li, Y.-T.; Sheng, Z.-M.; Zhang, X.-C. Strong Terahertz Radiation from a Liquid-Water Line. *Physical Review Applied* **2019**, *12*.

Zhao, Y.; Hwan Lee, J.; Zhu, Y.; Nazari, M.; Chen, C.; Wang, H.; Bernussi, A.; Holtz, M.; Fan, Z. Structural, Electrical, and Terahertz Transmission Properties of VO2 Thin Films Grown on c-, r-, and m-Plane Sapphire Substrates. *Journal of Applied Physics* **2012**, *111*, 053533